

---

# Silencing PCSK9 reshapes the spatiotemporal activation of STING for safe and effective cancer immunotherapy

---

---

Received: 30 June 2025

---

Accepted: 12 November 2025

---

Cite this article as: Sun, P., Han, F., Li, X. *et al.* Silencing PCSK9 reshapes the spatiotemporal activation of STING for safe and effective cancer immunotherapy. *Nat Commun* (2025). <https://doi.org/10.1038/s41467-025-66630-x>

Pengbo Sun, Fangping Han, Xinyan Li, Chengcheng Wu, Tingyue Deng, Jia He, Conggang Zhang & Rui Kuai

---

We are providing an unedited version of this manuscript to give early access to its findings. Before final publication, the manuscript will undergo further editing. Please note there may be errors present which affect the content, and all legal disclaimers apply.

If this paper is publishing under a Transparent Peer Review model then Peer Review reports will publish with the final article.

1 **Silencing PCSK9 reshapes the spatiotemporal activation of STING for safe and effective cancer  
2 immunotherapy**

3 Pengbo Sun<sup>1,2,#</sup>, Fangping Han<sup>1,2,#</sup>, Xinyan Li<sup>1,2</sup>, Chengcheng Wu<sup>1,2</sup>, Tingyue Deng<sup>3</sup>, Jia He<sup>1,2</sup>,  
4 Conggang Zhang<sup>1,2,\*</sup>, Rui Kuai<sup>1,2,\*</sup>

5 1 School of Pharmaceutical Sciences, Tsinghua University, Beijing 100084, China.

6 2 Tsinghua-Peking Center for Life Sciences, Beijing 100084, China.

7 3 Beijing Frontier Research Center for Biological Structure, School of Life Sciences, Tsinghua  
8 University, 100084 Beijing, China.

9 <sup>#</sup>These authors contributed equally.

10 \*Corresponding authors. Email: [cgzhang@tsinghua.edu.cn](mailto:cgzhang@tsinghua.edu.cn); [ruikuai@tsinghua.edu.cn](mailto:ruikuai@tsinghua.edu.cn)

11 **Abstract**

12 The cyclic GMP–AMP synthase (cGAS)–stimulator of interferon genes (STING) pathway is a central  
13 regulator of innate immunity and a promising target for cancer immunotherapy. However, the clinical  
14 translation of STING agonists is limited by suboptimal response rates and dose-limiting toxicities,  
15 particularly in the liver. These challenges highlight the presence of endogenous inhibitors of STING  
16 signaling and underscore the need for strategies that enable tissue-specific modulation of STING  
17 activity. Here, we identify proprotein convertase subtilisin/kexin type 9 (PCSK9), a key regulator of  
18 cholesterol metabolism, as a negative modulator of STING activation. Mechanistically, PCSK9  
19 competes with STING for binding to a shared cargo receptor, which is critical for STING trafficking.  
20 PCSK9 deficiency markedly enhances the immunostimulatory effects of STING agonists. Capitalizing  
21 on the elevated expression of PCSK9 in the liver relative to tumors, we develop a formulation that  
22 delivers a low-dose STING agonist alongside PCSK9-targeting siRNA, thereby achieving tumor-  
23 selective STING activation while minimizing hepatotoxicity. These findings reveal an unanticipated role  
24 for PCSK9 in innate immune regulation and establish a therapeutic approach to enhance the safety and  
25 efficacy of STING-based immunotherapies, with broader implications for other STING-associated  
26 modalities, including radiotherapy and chemotherapy.

27 **Introduction**

28 Against an invading pathogen, the body's first line of defense is the innate immune system, which  
29 recognizes foreign pathogens and initiates the appropriate adaptive immune response. As such, the  
30 innate immune system plays a crucial role in cancer therapeutics by shaping the tumor  
31 microenvironment and determining the therapeutic efficacy of treatments<sup>1</sup>. One important innate  
32 immune pathway is the cGAS-STING pathway<sup>2</sup>, whose activation produces various cytokines, including  
33 type I interferons that promote adaptive T cell-mediated antitumor immunity<sup>3-8</sup>.

34 While STING agonists have shown great initial success in preclinical studies<sup>9-11</sup>, they suffer from low  
35 objective response rates and severe adverse events, including exacerbated liver function in clinical  
36 trials<sup>12,13</sup>. These clinical challenges suggest the existence of key negative regulators of STING signaling,  
37 yet clinically translatable modulators remain elusive. Equally pressing is the need to selectively enhance  
38 STING activation within tumors while limiting off-target activation in the liver—a goal complicated by  
39 the ubiquitous expression of STING across tissues. Although various STING agonist-based cancer  
40 immunotherapies have been developed to enhance tumor-targeted drug delivery and improve therapeutic  
41 efficacy, they often accumulate in the liver, contributing to hepatic toxicity<sup>11,14</sup>. Thus, a strategy capable  
42 of reprogramming the spatiotemporal activation of STING is urgently needed.

43 Cholesterol has been shown to impair type I interferon responses in a STING-dependent manner<sup>15</sup>. One  
44 key regulator of cholesterol homeostasis is PCSK9, which is highly expressed in the liver<sup>16,17</sup>.

45 Interestingly, tumors also express PCSK9<sup>18</sup>, although at a lower level than the liver. Moreover,  
46 intratumoral PCSK9 levels negatively correlate with survival and type I interferon responses across  
47 multiple cancers<sup>19,20</sup>. These findings motivate us to hypothesize that PCSK9 may negatively regulate  
48 STING signaling. Importantly, because PCSK9 expression in the liver is higher than in tumors<sup>21</sup>, a  
49 formulation containing low-dose PCSK9 siRNA and STING agonists may completely knock down  
50 PCSK9 in the tumor to amplify STING activation, while the remaining PCSK9 in the liver can still  
51 suppress STING activation. These features will ultimately lead to enhanced therapeutic efficacy and  
52 reduced toxicity that can not be achieved by STING agonists alone.

53 Here, we demonstrate that PCSK9 is an endogenous suppressor in STING signaling. Mechanistically,  
54 the STING signaling involves the anterograde trafficking of STING from the endoplasmic reticulum  
55 (ER) to the Golgi apparatus, which requires surfeit locus protein 4 (SURF4), a bidirectional cargo  
56 receptor that mediates protein transport. PCSK9 competes with STING for binding to SURF4 during  
57 their anterograde trafficking and, therefore, limits STING signaling. These findings reveal a critical and  
58 multifaceted role for PCSK9 at the interface of maintaining metabolic and innate immune homeostasis,  
59 uncovering a rate-limiting mechanism in STING signal transduction. Strikingly, systemic administration  
60 of nanoparticles containing a low-dose STING agonist and PCSK9-siRNA induces potent antitumor  
61 immunity without inducing hepatic immune toxicity that is typically seen for STING agonists alone at  
62 the effective dose. Because PCSK9-siRNA has already been approved to treat hyperlipidemia<sup>16</sup>, we  
63 envision that our strategy may have immediate and broad clinical applications for cancer  
64 immunotherapy in the future.

65 **Results**

66 **PCSK9 silencing potentiates STING activation**

67 To initially explore the potential correlation between PCSK9 and innate immune signaling, we analyzed  
68 its mRNA expression alongside six immune-related genes in tumors from 42 rectal cancer patients  
69 (GEO: GSE15781, Fig. 1a)<sup>22</sup>. PCSK9 levels negatively correlate with IFN- $\beta$  or ISG20, but not with  
70 STING, Mitochondrial antiviral signaling protein (MAVS), IL-6, or IL-1 $\beta$  (Fig. 1b-g). These findings  
71 suggest that elevated PCSK9 expression may impair type I interferon responses, but this effect is not  
72 associated with the expression of key adaptor proteins (STING or MAVS).

73 To confirm whether PCSK9 affects STING activation, we treated bone marrow-derived dendritic cells  
74 (BMDCs) with a weak STING agonist<sup>23</sup> Mn<sup>2+</sup> and PCSK9-siRNA (siPCSK9) or control siRNA (siCtrl),  
75 and then measured IFN- $\beta$  production to assess STING activation. To reduce double-stranded RNA-  
76 induced immunostimulation, both siPCSK9 and siCtrl were chemically modified<sup>16</sup> in our study.  
77 Surprisingly, treating BMDCs with siPCSK9 and Mn<sup>2+</sup> (siPCSK9/Mn<sup>2+</sup>) induced a 40-fold increase in  
78 IFN- $\beta$  production. This effect was not observed in BMDCs treated with siCtrl/Mn<sup>2+</sup> (Fig. 1h, i). Mn<sup>2+</sup>

79 alone had an EC<sub>50</sub> of  $5.35 \pm 0.72$  mM, while combining with 10 or 20 µg/ml of siPCSK9 reduced the  
80 EC<sub>50</sub> to  $0.87 \pm 0.42$  mM and  $0.37 \pm 0.17$  mM, respectively. In contrast, Mn<sup>2+</sup> combined with siCtrl  
81 showed no increase in activity, confirming that the enhanced STING activation was PCSK9-dependent  
82 (Fig. 1j, k). BMDCs treated with siPCSK9/Mn<sup>2+</sup> and siCtrl/Mn<sup>2+</sup>, or THP1<sup>PCSK9 KO</sup> and THP1<sup>WT</sup> cells  
83 treated with Mn<sup>2+</sup>, showed similar levels of cGAMP (Supplementary Fig. 1a-b), indicating siPCSK9 did  
84 not change the ability of Mn<sup>2+</sup> to catalyze cGAS to produce cGAMP<sup>24</sup>. Moreover, mouse and human  
85 IFN reporter monocytes, including Raw264.7-Lucia ISG and THP1-Lucia ISG cells, exhibited stronger  
86 IFN responses upon exposure to siPCSK9/Mn<sup>2+</sup> (Fig. 1l, m). This pattern was further validated by  
87 combining siPCSK9 with other STING agonists such as c-di-AMP and cGAMP (Fig. 1n, o). These  
88 results indicate that PCSK9 plays an important role in limiting STING activation, and silencing PCSK9  
89 amplifies the activity of STING agonists. We also tested the PCSK9 antibody Evolocumab in BMDCs  
90 and found that it failed to enhance IFN-β production with either Mn<sup>2+</sup> or cGAMP (Supplementary Fig.  
91 2a-b).

## 92 **PCSK9 suppresses type I interferon production in a STING-dependent manner**

93 We next sought to understand whether PCSK9 regulates other innate immune pathways, such as the  
94 Toll-like receptor 3 and 4 (TLR3 and 4) pathways, which have also been shown to induce type I  
95 interferon secretion<sup>25</sup>. Interestingly, compared with siCtrl, siPCSK9 only slightly changed IFN response  
96 upon mixing with the TLR3 agonist Poly(I:C) (Fig. 2a-c) or TLR4 agonist Lipopolysaccharide (LPS)  
97 (Fig. 2d-e). Based on these results, PCSK9 appears to inhibit the STING signaling more substantially.  
98 Indeed, knocking out STING in BMDC abrogated the ability of siPCSK9/Mn<sup>2+</sup> to induce type I  
99 interferon secretion (Fig. 2f), and a similar pattern was observed in THP<sup>STING KO</sup> cells (Fig. 2g).  
100 Moreover, interferon-stimulated genes (*Ifnb*, *Cxcl10*, *Ccl5*, *ISG15*, *IFIT3*, and *TNFα*) were also  
101 substantially decreased in BMDC<sup>STING KO</sup> but not in BMDC<sup>WT</sup> (Fig. 2h-m). Altogether, these results  
102 indicate that PCSK9 restrains Mn<sup>2+</sup>-induced type I interferon responses in a STING-dependent manner.

## 103 **PCSK9 limits STING signaling by interfering with STING anterograde trafficking**

104 A key rate-limiting step in cGAS-STING signaling transduction is STING trafficking from the ER to the  
105 Golgi (anterograde trafficking)<sup>26-31</sup>. Thus, we next monitored the formation of STING puncta, a  
106 hallmark of trafficked STING on the Golgi, in HeLa<sup>WT</sup> and PCSK9-knockout HeLa (HeLa<sup>PCSK9 KO</sup>) cells  
107 under Mn<sup>2+</sup> stimulation. HeLa<sup>PCSK9 KO</sup> cells exhibited faster STING puncta formation than HeLa<sup>WT</sup> cells  
108 (Fig. 2n,o), suggesting PCSK9 deficiency promoted the anterograde STING trafficking.

109 We next sought to understand the mechanism by which PCSK9 regulates STING trafficking. Previous  
110 studies have shown that the anterograde STING trafficking was mediated by COP II vesicles, and the  
111 retrograde STING trafficking from Golgi to ER was mediated by COP I vesicles to maintain the delicate  
112 balance and avoid autoimmunity<sup>32,33</sup>. Moreover, SURF4 on the COP I vesicle was responsible for  
113 binding to STING and facilitating the retrograde trafficking<sup>32,34-36</sup>. Interestingly, SURF4 on the COP II  
114 vesicles also mediates the anterograde trafficking of various secretory proteins<sup>37</sup>, including PCSK9<sup>38</sup>. In  
115 light of these observations, we hypothesized that SURF4 might also mediate anterograde trafficking of  
116 STING, and PCSK9 might compete with STING for binding to SURF4, thereby limiting the anterograde  
117 transport of STING in COPII vesicles.

118 To confirm the role of SURF4 in STING anterograde trafficking, we generated SURF4-overexpressing  
119 HeLa (HeLa<sup>SURF4 OE</sup>) and SURF4-knockout HeLa (HeLa<sup>SURF4 KO</sup>) cells. After cGAMP stimulation, we  
120 observed strong colocalization of STING with SURF4, and anterograde STING trafficking was  
121 enhanced in HeLa-hSTING<sup>SURF4 OE</sup> cells (Supplementary Fig. 3a-b). Moreover, cGAMP treatment  
122 induced stronger STING activation in THP1<sup>SURF4 OE</sup> and 293T<sup>SURF4 OE</sup> cells (Supplementary Fig. 3c-d).  
123 In contrast, SURF4-knockout HeLa cells exhibited impaired STING and PCSK9 anterograde trafficking  
124 and reduced STING signaling activation compared to HeLa<sup>WT</sup> or HeLa<sup>SURF4 OE</sup> cells. Meanwhile, a basal  
125 activation of STING was also observed in SURF4-knockout cells (Supplementary Fig. 3e-j). These  
126 results indicate that SURF4 is involved not only in the retrograde trafficking of STING but also in the  
127 anterograde trafficking and activation of STING.

128 To directly analyze this possible vesicle transport-mediated signaling crosstalk, we investigated the  
129 intracellular distribution of PCSK9 and STING in HeLa cells. Interestingly, the enhanced STING

130 anterograde trafficking appears to be associated with decreased PCSK9 transport, as measured by  
131 counting fluorescence antibody-labeled PCSK9 protein puncta (dots) (Fig. 2p). PCSK9 was strongly  
132 colocalized with GFP-labeled STING in a vesicle-like structure upon STING activation (Fig. 2q).  
133 Further immunostaining analysis confirmed that the vesicle-like structure contained SEC24 Homolog B  
134 (Sec24B) (Fig. 2r), a hallmark of COPII vesicles<sup>37,39</sup>, indicating that PCSK9 and STING are co-  
135 packaged and transported by COPII vesicles. The observed changes in STING trafficking were  
136 positively associated with the activation of cGAS-STING signaling, as evidenced by the stronger  
137 activation of phospho-STING (Ser366) and phospho-TBK1 (Ser172) following STING agonist  
138 treatment. Moreover, the unchanged expression of STING and SURF4 further suggests that PCSK9  
139 restricts STING signaling by modulating its anterograde trafficking efficiency (Fig. 2s-t).

#### 140 **PCSK9 limits STING anterograde trafficking through competitive binding to SURF4**

141 We next investigated the interactions among STING, PCSK9, and SURF4. THP1<sup>PCSK9 KO</sup>, L929<sup>PCSK9 KO</sup>,  
142 and HeLa<sup>PCSK9 KO</sup> cells exhibited faster and stronger STING/TBK1/IRF3 phosphorylation than the  
143 corresponding wild-type cells upon exposure to low-dose STING agonists (Mn<sup>2+</sup> or cGAMP) (Fig. 3a-  
144 d). We also found increased STING phosphorylation at early time points in THP1<sup>PCSK9 KO</sup> cells  
145 following cGAMP treatment (Supplementary Fig. 4). We further assessed the kinetics of STING puncta  
146 formation in HeLa cells by confocal microscopy under the treatment of a low concentration of cGAMP.  
147 STING puncta formed rapidly within 60 minutes in HeLa<sup>PCSK9 KO</sup> cells, while in HeLa<sup>WT</sup> cells, it took at  
148 least 120 minutes (Fig. 3e), which is consistent with the pattern of STING signaling activation in Fig.  
149 3d. In contrast, the overexpression of PCSK9 (OE) significantly inhibited STING activation in THP1  
150 cells at 0.5, 1, 2, and 4 hours after cGAMP treatment, compared to THP1<sup>WT</sup> cells (Fig. 3f). Similarly,  
151 cGAMP or plasmid-induced cGAS-STING activation was also significantly reduced by transfection  
152 with different doses (1.5 to 5 µg) of PCSK9 plasmids (Fig. 3g, Supplementary Fig. 5a). These results  
153 indicate that PCSK9 inhibits STING anterograde trafficking from the earliest stages and throughout the  
154 entire process, likely by affecting the initiation of SURF4-mediated COPII vesicle assembly.

To investigate the potential interaction among PCSK9, SURF4, and STING, we conducted a competitive binding and inhibition assay in HEK293T cells. Here, PCSK9 transfection significantly inhibited the cGAMP-induced STING activation. By contrast, SURF4 expression promoted cGAMP-induced STING activation, which is impaired by PCSK9 overexpression in SURF4-transfected HEK293T cells (Fig. 3h). Next, we compared the effects of SURF4 overexpression and PCSK9 knockout on STING activation in THP1 cells with the same cGAMP stimulation using the IFN reporter assay. Overexpressing SURF4 induced stronger STING activation than knocking out PCSK9, suggesting that adequate SURF4 can counteract the inhibitory effect of PCSK9 on STING signaling (Fig. 3i). Similarly, SURF4 and STING-transfected HEK293T cells also showed enhanced cGAS-STING activation upon cGAMP treatment (Fig. 3j). However, this enhanced activation was abolished in HEK293T cells that received the same treatment but without STING transfection, confirming that this process is STING-dependent (Supplementary Fig. 5b). The co-immunoprecipitation (Co-IP) revealed that in the process of STING activation and anterograde trafficking, PCSK9 competitively interacts with STING, ultimately preventing STING from binding to SURF4. We observed the stronger binding of SURF and STING, both in siPCSK9/Mn<sup>2+</sup>-treated BMDC (Fig. 3k) and cGAMP-treated THP1<sup>PCSK9 KO</sup> cells (Fig. 3l). Notably, HeLa<sup>PCSK9 KO</sup> cells and THP1<sup>PCSK9 KO</sup> cells had similar levels of intracellular cholesterol compared with their WT counterparts (Supplementary Fig. 6a-b), thus excluding the potential influence of cholesterol on STING activation<sup>40</sup>.

To further explain our findings, molecular dynamics (MD) simulations of the SURF4-STING and SURF4-PCSK9 complexes (Fig. 3m) revealed a lower binding free energy ( $\Delta G_{bind} = -324$  kJ/mol) for the SURF4-PCSK9 complex, suggesting a more favorable interaction compared to the SURF4-STING complex ( $\Delta G_{bind} = -218$  kJ/mol) (Fig. 3n). Further analysis identified a steric clash when both PCSK9 and STING bind to SURF4 simultaneously (Fig. 3o). Additionally, AlphaFold2-predicted structures of human and mouse SURF4, PCSK9, and STING dimers showed high similarity across species (Supplementary Fig. 7). AlphaFold3 predictions for the SURF4-PCSK9 and SURF4-STING complexes revealed similar binding patterns in both species, with high confidence ( $pTM > 0.5$ ) (Supplementary Fig.

181 8 and 9). However, pTM scores for the SURF4-PCSK9-STING ternary complexes were below 0.5,  
182 suggesting the instability and low likelihood of ternary complex formation (Supplementary Fig. 10).  
183 Altogether, the above results indicate that PCSK9 negatively regulates the cGAS-STING pathway by  
184 competitively binding to SURF4 and limiting STING anterograde trafficking (Supplementary Fig. 11).

185 **Nanoparticles containing PCSK9 siRNA and STING agonists enable safe and effective cancer  
186 immunotherapy**

187 Given the promising results and mechanistic rationale of amplified cGAS-STING signaling following  
188 PCSK9 silencing, we sought to translate this effect into a viable therapeutic approach. To this end, we  
189 developed a facile method for encapsulating siPCSK9 and STING agonists (e.g., Mn<sup>2+</sup> or cGAMP) into  
190 hyaluronic acid (HA)-coated lipid nanoparticles<sup>11,41</sup> (Fig. 4a, Supplementary Fig. 12a). Dynamic light  
191 scattering (DLS) showed that NP<sup>siPCSK9/cGAMP</sup> had an average diameter of 66 nm (Fig. 4b, Supplementary  
192 Fig. 12b). The encapsulation efficiency was over 95% for siPCSK9 and approximately 10% for cGAMP  
193 (Supplementary Fig. 12c,d). The sizes and encapsulation efficiencies of NP<sup>cGAMP</sup> and NP<sup>siPCSK9</sup> were  
194 comparable to those of NP<sup>siPCSK9/cGAMP</sup> (Supplementary Fig. 12e,f). Additionally, we used a similar  
195 method to prepare NP<sup>siPCSK9/Mn<sup>2+</sup></sup>, which had a size and structure similar to NP<sup>siPCSK9/cGAMP</sup>  
196 (Supplementary Fig. 12g), with Mn<sup>2+</sup> exhibiting a pH-responsive release profile due to its pH-dependent  
197 binding to siRNA (Supplementary Fig. 12h). We next analyzed the in vitro activity of these  
198 nanoparticles. As expected, NP<sup>siPCSK9/cGAMP</sup> and NP<sup>siPCSK9/Mn<sup>2+</sup></sup> showed significantly enhanced IFN- $\beta$   
199 release compared to their respective controls (Supplementary Fig. 12i-j), suggesting that siPCSK9  
200 significantly potentiates the effect of low-dose STING agonists. Cryo-EM analysis revealed that  
201 NP<sup>cGAMP</sup> had one lipid bilayer, whereas NP<sup>siPCSK9</sup> and NP<sup>siPCSK9/cGAMP</sup> exhibited two lipid bilayers (Fig.  
202 4c, Supplementary Fig. 13). This structural difference was likely due to the strong negative charge of  
203 siRNA, which influences lipid organization. RNA-seq analysis revealed that NP<sup>siPCSK9/cGAMP</sup> treatment  
204 broadly activated the cGAS-STING signaling-related genes in BMDCs (Fig. 4d, Supplementary Fig.  
205 14a-d). Moreover, the expression of structural proteins related to COPI and COPII vesicles was similar

206 for NP<sup>cGAMP</sup> and NP<sup>siPCSK9/cGAMP</sup> (Supplementary Fig. 14e), thus excluding the effect of vesicle number  
207 on STING trafficking.

208 Intravenously injected hyaluronic acid-coated nanoparticles accumulated in the tumor as early as 1 h and  
209 remained for over 72 h (Supplementary Fig. 15a), indicating these nanoparticles are suitable for in vivo  
210 therapeutic studies. A single dose of NP<sup>siPCSK9/cGAMP</sup> led to complete tumor regression in 100% of treated  
211 mice, while NP<sup>siPCSK9</sup> or NP<sup>cGAMP</sup> failed to inhibit tumor growth (Fig. 4e-g, Supplementary Fig. 16a-c).  
212 Notably, animals cured with NP<sup>siPCSK9/cGAMP</sup> were protected from rechallenge with MC38 cells (Fig. 4h).  
213 NP<sup>siCtrl/cGAMP</sup> failed to inhibit tumor growth (Supplementary Fig. 17a, b), further indicating the enhanced  
214 therapeutic effect was PCSK9-dependent. Combination of the PCSK9 antibody Evolocumab and  
215 NP<sup>siCtrl/cGAMP</sup> also failed to inhibit tumor growth (Supplementary Figure 18), implying that blocking  
216 extracellular PCSK9 does not affect the STING activation. Moreover, NP<sup>siPCSK9/cGAMP</sup> lost the  
217 therapeutic effect in C57BL/6<sup>STING-/-</sup> mice bearing MC38<sup>WT</sup> tumor cells (Supplementary Fig. 19a-c), but  
218 it maintained the strong therapeutic effect in C57BL/6<sup>WT</sup> mice bearing MC38<sup>STING-/-</sup> tumor cells  
219 (Supplementary Fig. 19d-g), suggesting that host STING signaling plays a critical role in NP<sup>siPCSK9/cGAMP</sup>  
220 treatment. The immune cell depletion in C57BL/6 or C57BL/6<sup>Batf3-/-</sup> mice revealed that dendritic cells,  
221 macrophages, NK, CD4<sup>+</sup>, and CD8<sup>+</sup> T cells all contributed to the therapeutic effect (Fig. 4i-j).  
222 A single dose of NP<sup>siPCSK9/cGAMP</sup> induced higher levels of mature dendritic cells (mDCs), M1  
223 macrophages, cytotoxic CD8<sup>+</sup> T lymphocytes, and natural killer (NK) cells within the tumor  
224 microenvironment compared with other groups. In contrast, the frequencies of immune-suppressive  
225 regulatory T cells (Tregs) and myeloid-derived suppressor cells (MDSCs) were significantly reduced in  
226 the NP<sup>siPCSK9/cGAMP</sup> group compared to control nanoparticles (Fig. 4k-n, Supplementary Fig. 20a-h).  
227 Additionally, NP<sup>siPCSK9/cGAMP</sup> induced a marked increase in OVA-specific CD8<sup>+</sup> T cells (SIINFEKL) in  
228 the MC38-OVA model (Fig. 4o, Supplementary Fig. 20i-j), indicating enhanced priming and expansion  
229 of cytotoxic T lymphocytes (CTLs). Similarly, NP<sup>siPCSK9/Mn<sup>2+</sup></sup> induced stronger antitumor responses than  
230 control groups (Supplementary Fig. 21-23).

231 Notably, a single-dose systemic administration of NP<sup>siPCSK9/cGAMP</sup> (1.5 µg/dose cGAMP) achieved not  
232 only potent antitumor effects but also exhibited excellent safety profiles, without body weight changes at  
233 24 and 48 hours post-administration (Fig. 5a-c). In contrast, NP<sup>cGAMP</sup> at the effective dose (5 µg/dose)  
234 induced over 15% body weight loss at 24 hours post intravenous administration, although this dose also  
235 induced robust antitumor immune responses and therapeutic effects. It should be noted that lower doses  
236 (1.5 µg and 2.5 µg/dose cGAMP) of NP<sup>cGAMP</sup> failed to show strong therapeutic effects.

237 We next evaluated the therapeutic efficacy and safety of systemic NP<sup>siPCSK9/cGAMP</sup> and NP<sup>cGAMP</sup> in the  
238 MDA-MB231 xenograft models. A single dose of NP<sup>siPCSK9/cGAMP</sup> resulted in complete tumor regression  
239 in 100% of treated mice without significant weight loss. In contrast, high-dose NP<sup>cGAMP</sup> failed to induce  
240 tumor regression in any of the six animals and caused significant weight loss (>15%) at 24 h post-  
241 administration (Fig. 5d-i). Moreover, combining NP<sup>siPCSK9/cGAMP</sup> with αPD-L1 resulted in complete  
242 tumor remission in five out of six B16F10 tumor-bearing mice, without significant body weight loss  
243 (Fig. 5j-o). Altogether, these results indicate that a low dose of NP<sup>siPCSK9/cGAMP</sup> is highly effective and  
244 safe for cancer immunotherapy, while NP<sup>cGAMP</sup> was only effective at a relatively high dose that induces  
245 severe side effects.

#### 246 **NP<sup>siPCSK9/cGAMP</sup> induces stronger STING activation in the tumor than in the liver**

247 NP<sup>siPCSK9/cGAMP</sup> and high-dose NP<sup>cGAMP</sup> had similar biodistribution profiles at 24 hours post  
248 administration, with both formulations demonstrating ~80% liver accumulation (Supplementary Fig.  
249 24a-c), indicating the liver may experience stronger off-target STING activation than other organs.  
250 However, the liver has a higher basal level of PCSK9 than the tumor (Fig. 6a), making it possible to  
251 silence PCSK9 for achieving differential activation of STING in the liver and tumor. Interestingly,  
252 NP<sup>siPCSK9/cGAMP</sup> induced a significantly lower liver IFN-β production and serum AST (the liver injury  
253 marker) than high-dose NP<sup>cGAMP</sup> between 12 and 72 hours (Fig. 6b-c). Moreover, NP<sup>siPCSK9/cGAMP</sup>  
254 induced a lower serum IFN-β than NP<sup>cGAMP</sup>, although IFN-β in the spleen was similar. Compared with  
255 NP<sup>cGAMP</sup>, NP<sup>siPCSK9/cGAMP</sup> induced a slightly higher peak concentration of IFN-β, which remained in the  
256 tumor for about 72 h (Supplementary Fig. 25a-c). In parallel with these changes, NP<sup>siPCSK9/cGAMP</sup> did not

257 induce inflammation or vascular damage in the liver, but high-dose NP<sup>cGAMP</sup> induced large areas of  
258 inflammatory damage in the liver, including inflammation in the hepatic artery and portal vein (Fig. 6d,  
259 Supplementary Fig. 26). Meanwhile, NP<sup>siPCSK9/cGAMP</sup> treatment induced more extensive inflammatory  
260 damage and erythrocyte infiltration in the tumor than NP<sup>cGAMP</sup> (Fig. 6e, Supplementary Fig. 27).  
261 Additionally, NP<sup>siPCSK9/cGAMP</sup> and high-dose NP<sup>cGAMP</sup> treatments exhibited no difference in the  
262 recruitment of immune cells to the periarteriolar lymphoid sheaths surrounding the splenic arterioles  
263 (Supplementary Fig. 28).

264 We next sought to understand the mechanism underlying the differential STING activation in the liver  
265 and tumor. Low-dose NP<sup>siPCSK9/cGAMP</sup> almost completely knocked down PCSK9 in the tumor to amplify  
266 STING activation, while the liver still had remaining PCSK9 to suppress STING activation (Fig. 6f-g).  
267 This is because the liver has a higher basal level of PCSK9 than the tumor. Although high-dose  
268 NP<sup>cGAMP</sup>-treated mice also had PCSK9 in the liver, PCSK9 failed to fully suppress the STING activation  
269 as ~80% of the high-dose NP<sup>cGAMP</sup> was in the liver (Fig. 6f). Moreover, NP<sup>cGAMP</sup>-treated mice had  
270 intratumoral PCSK9 that suppressed the STING activation, as shown by the lower level of  
271 phosphorylated STING and TBK1 (Fig. 6g). The proposed working model is presented in Fig. 6h. The  
272 single-cell sequencing data (sourced from the Human Protein Atlas<sup>42</sup>) revealed high PCSK9 expression  
273 in hepatocytes and liver-resident macrophages (Kupffer cells) (Supplementary Fig. 29a). In line with  
274 this, both CD45<sup>+</sup> and CD45<sup>-</sup> cells exhibited high PCSK9 in the liver. As a result, NP<sup>siPCSK9/cGAMP</sup> only  
275 partially reduced PCSK9 and exhibited less STING activation compared with the therapeutically  
276 effective dose of NP<sup>cGAMP</sup>. In the tumor, CD45<sup>+</sup> cells showed stronger STING phosphorylation after  
277 NP<sup>siPCSK9/cGAMP</sup> treatment, whereas CD45<sup>-</sup> cells displayed a similar but less pronounced trend  
278 (Supplementary Fig. 29b). Interestingly, the structures of PCSK9, STING, and SURF4 were conserved  
279 across different species (Fig. 7), suggesting that the inhibition of STING trafficking by PCSK9 may be  
280 an ancient and evolutionarily conserved regulatory process. These results suggest that the patterns  
281 identified in mice may be relevant for future clinical trials, supporting the potential clinical translation of  
282 our findings.

283 **Discussion**

284 Our findings reveal that PCSK9 inhibits activation of the cGAS–STING pathway by restricting  
285 anterograde trafficking of STING from the endoplasmic reticulum to the Golgi apparatus. This  
286 mechanism not only offers a potential explanation for the limited clinical efficacy of STING agonists  
287 but also suggests a strategy to unlock their therapeutic potential for safe and effective cancer  
288 immunotherapy. While recent studies have shown that targeting extracellular PCSK9 enhances tumor  
289 cell-surface MHC I stability<sup>43</sup>, the role of intracellular PCSK9 in regulating innate immunity has  
290 remained largely unexplored. Our study addresses this gap and underscores the multifaceted functions of  
291 PCSK9 across innate and adaptive immune responses.

292 Moreover, we demonstrate that co-delivery of siPCSK9—an FDA-approved therapeutic—with a low-  
293 dose STING agonist via bioengineered nanoparticles markedly enhances antitumor efficacy. This  
294 approach may help overcome key barriers that have hampered STING agonist-based therapies,  
295 providing a broadly applicable and translationally feasible strategy for cancer immunotherapy.  
296 Furthermore, this 'biological switch-like' strategy for tissue-specific immune modulation may also have  
297 broad applications in radiotherapy and chemotherapy, both of which involve STING activation.

298 **Methods**299 **Ethics statement**

300 All animal experiments were in accordance with and approved by the University Committee on Use and  
301 Care of Animals at Tsinghua University (Approved Animal Protocol 22-KR-1). Animals were  
302 euthanized when the tumor reached 15 mm in any dimension or when they became moribund with  
303 severe weight loss (defined as >20% body weight loss) or unhealing ulceration. This limit was not  
304 exceeded at any point.

305 **Preparation of immature BMDCs**

306 Bone marrow-derived dendritic cells (BMDCs) were isolated by flushing the femur and tibia from  
307 C57BL/6 or C57BL/6<sup>STING<sup>-/-</sup></sup> mice and cultured in RPMI 1640 media (Gibco) supplemented with 10%  
308 FBS (Biological Industry (BI)), 1% penicillin/streptomycin (Gibco), 20 ng/ml of GM-CSF (Genscript),

309 and 50  $\mu$ M  $\beta$ -mercaptoethanol at 37 °C and 5% CO<sub>2</sub>. Half of the medium was removed and  
310 supplemented with 20 ng/ml GM-CSF-containing medium on days 3 and 6, and the non-adherent cells  
311 were harvested on day 7 and used immediately.

312 **Synthesis of siRNA**

313 The sequence and modification of PCSK9 and Ctrl siRNA were designed as described previously <sup>16</sup>.  
314 siRNA was customized from General Biol. (Anhui) Co., Ltd. The synthesis and deprotection of  
315 Oligonucleotides were carried out with a standard solid-phase synthesis procedure. Then, single-  
316 stranded RNAs were purified from crude oligonucleotides by reversed-phase HPLC. Double-stranded  
317 siRNAs were generated by annealing equal amounts of sense and antisense strands.

318 **Preparation of NP containing siRNA and/or STING agonist**

319 The hyaluronic acid-coated lipid nanoparticle (NP) formulation was prepared by using a microfluidic  
320 device (INano<sup>TM</sup> E, Micro&Nano, Shanghai, China) to mix the ethanol phase containing selected lipids  
321 and aqueous phase containing selected siRNA and/or STING agonists. Briefly, to obtain the lipid-  
322 containing ethanol phase, 60.84 mM 1,2-Dioleoyl-3-trimethylammonium-propane chloride (DOTAP),  
323 57.12 mM 1,2-Dioleoyl-sn-glycero-3-phosphoethanolamine (DOPE), and 5.35 mM 1,2-distearoyl-sn-  
324 glycero-3-phosphoethanolamine-N-[methoxy(polyethylene glycol)-2000] (DSPE-PEG2000) (all  
325 purchased from AVT Pharmaceutical Tech Co., Ltd, Shanghai) were dissolved in ethanol. To obtain the  
326 aqueous phase, 100-500  $\mu$ g/ml siPCSK9 or siCtrl was dissolved in sterile normal saline (for NP<sup>siPCSK9</sup> or  
327 NP<sup>siCtrl</sup> preparation); or 100-500  $\mu$ g/ml siPCSK9 or siCtrl, and 20 mM MnCl<sub>2</sub> (Sigma, Cat#M3634) were  
328 dissolved in sterile normal saline (for NP<sup>siPCSK9/Mn2+</sup> and NP<sup>siCtrl/Mn2+</sup> preparation); or 100-500  $\mu$ g/ml  
329 siPCSK9 and 40  $\mu$ g/ml cGAMP (MCE, Cat# HY-100564) were dissolved in sterile normal saline (for  
330 NP<sup>siPCSK9/cGAMP</sup> preparation). The ethanol phase containing indicated lipids and the aqueous phase  
331 containing indicated molecules were mixed at a volume ratio of 3:1 (aqueous: ethanol) via the  
332 microfluidic device at a flow rate of 8 ml/min for nanoparticle production. Finally, the hyaluronic acid  
333 (HA) was added dropwise into the prepared liposome under constant vortexing to achieve a final HA  
334 concentration of 1 mg/ml, followed by dialysis for 4-6 h in normal saline at 4°C to remove ethanol and

335 unloaded molecules. NP<sup>Blank</sup>, NP<sup>Mn<sup>2+</sup></sup>, and NP<sup>cGAMP</sup> were all prepared using the same methods by  
336 adjusting the content of the aqueous phase accordingly. All NP formulations were sterilized through a  
337 220 nm filter before use.

338 To simplify the in vitro mechanism study, all siRNAs used in Figures 1-3 were delivered by HA-coated  
339 nanoparticles (NP): namely, NP<sup>siPCSK9</sup> was used in the siPCSK9 group, and NP<sup>siCtrl</sup> was used in the siCtrl  
340 group, with STING agonists physically mixed with these NP formulations for in vitro studies. However,  
341 to facilitate the codelivery of siRNA and STING agonists in vivo. All the siRNA and STING agonists  
342 were encapsulated into NP for in vivo use.

343 **Antibodies and reagents**

344 Rabbit antibodies against p-TBK1 (#5483), STING (#13647), p-STING (#19781), p-IRF3 (#4947),  
345 Golgin-97 (#13192S), Sec24B (#12042), and GAPDH (#5174) were purchased from Cell Signaling  
346 Technology. Rabbit antibodies against SURF4(#PA5-110450) were purchased from Thermofisher.  
347 Rabbit antibodies against PCSK9 (#Ab185194) were purchased from Abcam. Rabbit antibodies against  
348 PCSK9 (#A21909, A24478) were purchased from ABclonal Technology. Antibodies against Tubulin  
349 (HC101-01) and GADPH (HC301-01) were obtained from TransGen biotech.  
350 LPS (L3024) was purchased from Sigma. Human IFN- $\beta$  bioluminescent ELISA kit (luex-hifnbv2), 2'3'-  
351 cGAMP (tlrl-nacga23), and c-di-AMP (tlrl-nacda) were purchased from InvivoGen. Polyethylenimine  
352 (PEI, #23966-2) was obtained from Polysciences. Poly (I: C) LMW (#tlrl-picw-250) was purchased  
353 from Invivogen.

354 **Cell culture and treatment**

355 Throughout the studies, all cells were tested negative for mycoplasma contamination and  
356 morphologically confirmed. THP1-Lucia ISG cells (InvivoGen, No. thpl-isg) and THP1-Lucia NF- $\kappa$ B  
357 Cells (InvivoGen, No. thpl-nfkb) were cultured in RPMI 1640 medium (Gibco) supplemented with 10%  
358 (v/v) fetal bovine serum (FBS, Gemini), 1% (v/v) penicillin (100 U/ml, Solarbio), and streptomycin (100  
359  $\mu$ g/ml, Solarbio). Raw264.7 (ATCC, TIB-71), HEK293T cells (ATCC, CRL-3216), HeLa cells (ATCC,  
360 CCL-2), and L929 cells (ATCC, CCL-1) were cultured in Dulbecco's Modified Eagle's Medium

361 (DMEM, Gibco) containing 10% FBS and penicillin-streptomycin. All these cells mentioned above  
362 were maintained in a humidified incubator containing 5% CO<sub>2</sub> at 37 °C. To facilitate cGAMP delivery in  
363 vitro, perfringolysin O (PFO, 0.02 µg/mL) was utilized to improve the entry of the indicated  
364 concentrations of cGAMP into HeLa, HEK293T, and L929 cells. After treatment, cells were incubated  
365 at 37 °C with 5% CO<sub>2</sub> for 24 h for the Luciferase reporter assay. For western blotting, cells were treated  
366 and cultured for the indicated lengths of time, as shown in the figure legends.

367 **Construction of stable cell lines**

368 To generate stable cell lines overexpressing SURF4 or PCSK9, human *Surf4* and *Pcsk9* genes were  
369 inserted into the pCDH-CMV-MCS-IRES vector, followed by virus packing and lentiviral plasmid  
370 transduction of parent cells described below. To generate PCSK9-knockout L929 cells, PCSK9-  
371 knockout THP1-Lucia ISG, SURF4-knockout THP1-Lucia ISG, PCSK9-knockout HeLa-hSTING-GFP  
372 cells, PCSK9-knockout-HeLa-hSTING cells, SURF4-knockout HeLa-hSTING cells, or SURF4-  
373 knockout HeLa-hSTING-110GFP cells, the parent cells were transduced by lentiviral plasmids  
374 consisting of gRNA and plentiCRISPR v2 (Addgene Plasmid). For virus packaging, 14 µg of  
375 constructed plasmids with the two packaging plasmids psPAX2 (6 µg) and pMD2.G (4 µg) were co-  
376 transfected into HEK293T cells by the PEI transfection reagent. After 72 h, the supernatant was  
377 collected and filtered through a 0.22-µm membrane filter. The filtrate was then added to the indicated  
378 cells with polybrene (Sigma Aldrich) for another 48 h. The transfected cells were selected by 2 µg/ml  
379 puromycin or 5 µg/ml blasticidin (Thermo Fisher Scientific), determined by the selection markers on the  
380 plentiCRISPR backbone. The purified cells were used for further western blotting or immunostaining.  
381 All gRNA sequences for gene knockout and primer sequences for gene overexpression are provided in  
382 Supplementary Tables S1 and S2. The gRNA demonstrating optimal knockout efficiency, as determined  
383 by functional screening, are indicated in bold, and the corresponding knockout cell lines generated with  
384 these gRNAs were used for subsequent experiments.

385 **Enzyme-linked immunosorbent assay (ELISA)**

386 For human IFN- $\beta$  detection after PCSK9 silencing, THP1 cells were seeded in 12-well plates and treated  
387 with formulations containing 7.5  $\mu$ g/ml siCtrl or 7.5  $\mu$ g/ml siPCSK9 or 10  $\mu$ g/ml Poly (I: C) (transfected  
388 with PEI), or indicated combinations and incubated for 24 h at 37°C in 5% CO<sub>2</sub>. Then the supernatant  
389 was collected and the concentration of secreted IFN- $\beta$  was measured by the human IFN- $\beta$   
390 bioluminescent ELISA kit following the manufacturer's instructions. The optical density (OD) in each  
391 well was read at 450 nm.

392 For murine IFN- $\beta$  detection after PCSK9 silencing, BMDCs seeded in 96-well plates were treated with  
393 siCtrl or siPCSK9 (10 and 20  $\mu$ g/ml), or Mn<sup>2+</sup> (0-1600  $\mu$ M), or indicated combinations for 24 h. In some  
394 experiments, BMDCs were seeded in 96-well plates and treated with 20  $\mu$ g/ml siCtrl or siPCSK9, or 10  
395  $\mu$ g/ml Poly(I: C) (transfected with PEI) alone, or indicated combinations for 24 h. The supernatant was  
396 collected, and the concentration of secreted IFN- $\beta$  was measured by the LumiKine™ Xpress mIFN- $\beta$  2.0  
397 (InvivoGen, Cat# luex-mifnbv2) following the manufacturer's instructions.

398 To assess the cGAS-STING pathway activation induced by siRNA and STING agonists co-delivered by  
399 nanoparticles (NP). BMDCs were seeded in 96-well plates and treated with NP<sup>Blank</sup>(Blank vesicle),  
400 NP<sup>Mn<sup>2+</sup></sup> (NP containing 400  $\mu$ M Mn<sup>2+</sup>), NP<sup>cGAMP</sup> (NP containing 100 nM cGAMP), NP<sup>siCtrl</sup> (NP  
401 containing 20  $\mu$ g/ml siCtrl), NP<sup>siPCSK9</sup> (NP containing 20  $\mu$ g/ml siPCSK9 ), NP<sup>siCtrl/Mn<sup>2+</sup></sup> (NP containing  
402 20  $\mu$ g/ml siCtrl and 400  $\mu$ M Mn<sup>2+</sup>), NP<sup>siPCSK9/Mn<sup>2+</sup></sup> (NP containing 20  $\mu$ g/ml siPCSK9 and 400  $\mu$ M  
403 Mn<sup>2+</sup> ), andNP<sup>siPCSK9/cGAMP</sup> (NP containing 20  $\mu$ g/ml siPCSK9 and 100 nM cGAMP ) for 24 h. The  
404 supernatant was collected, and the concentration of secreted IFN- $\beta$  was measured by the LumiKine™  
405 Xpress mIFN- $\beta$  2.0 (InvivoGen, Cat# luex-mifnbv2).

#### 406 Luciferase reporter assay

407 THP1-Lucia ISG cells are derived from THP1 cells by stably transfecting the luciferase reporter gene  
408 under the control of interferon-stimulated response elements (ISRE). THP1-Lucia NF- $\kappa$ B cells were  
409 derived from THP1 cells by stably integrating the NF- $\kappa$ B-inducible Luc reporter element for monitoring  
410 the NF- $\kappa$ B activation. RAW-Lucia ISG cells were derived from Raw264.7 cells. For the luciferase  
411 assay, THP1-Lucia ISG, STING<sup>CRISPR/-</sup> THP1-Lucia ISG, and RAW-Lucia ISG cells were seeded in 96-

412 well plates at a density of  $3 \times 10^6$  cells/well and treated with 50  $\mu\text{M}$  Mn<sup>2+</sup> with or without 7.5  $\mu\text{g}/\text{ml}$   
413 NP<sup>siPCSK9</sup> at 37°C for 24 h. Then, 20  $\mu\text{l}$  cell suspension was mixed with 60  $\mu\text{l}$  luciferase buffer (50 mM  
414 NaCl, 50 mM HEPES pH 7.0, 10 mM EDTA, 0.05% CHAPS, 1  $\mu\text{M}$  Coelenterazine) and incubated in  
415 darkness for 5 min at room temperature. Luminescence was measured by Cytatio3™ Cell Imaging  
416 Reader (BioTek).

417 THP1-Lucia ISG cells were also treated with another two STING agonists (1  $\mu\text{M}$  cGAMP, 10  $\mu\text{M}$  c-di-  
418 AMP) or TLR agonists (500 ng/ml LPS, 10  $\mu\text{g}$  Poly(I: C)) with or without 7.5  $\mu\text{g}/\text{ml}$  siCtrl or siPCSK9  
419 at 37°C for 24 h. THP1-Lucia NF-κB cells were treated with 500 ng/ml LPS and/or siCtrl or siPCSK9.  
420 The luciferase reporter activity was determined following the standard protocol.

#### 421 **RNA isolation and quantitative RT-PCR**

422 BMDCs were treated with 400  $\mu\text{M}$  Mn<sup>2+</sup> or 20  $\mu\text{g}/\text{ml}$  siCtrl or siPCSK9 for 24 h. Total RNA was  
423 extracted by M5 HiPer Total RNA Extraction Reagent (MF034-01, Mei5 Biotechnology) according to  
424 the manufacturer's protocol. Then, 1  $\mu\text{g}$  RNA was reverse transcribed into cDNA by utilizing the M5  
425 Super plus qPCR RT kit (MF166-plus-01, Mei5 Biotechnology). Real-time quantitative PCR was  
426 performed using HiPer SYBR Premix EsTaq (MF787-T, Mei5 Biotechnology). The primer sequences  
427 detecting the indicated genes are shown in Table S3. All the indicated siRNA we used in this study were  
428 delivered by HA-coated nanoparticles (NP) as described above.

#### 429 **Western blotting**

430 Cells were lysed by lysis buffer (20 mM Tris-HCl, 150 mM NaCl, 10% glycerol, 1% Triton X-100,  
431 0.1% SDS, 1 mM EDTA-Na<sub>2</sub>, 1 mM Na<sub>3</sub>VO<sub>4</sub>, 25 mM β-glycerophosphate) supplemented with 0.5%  
432 PMSF and 0.05% Leupeptin on ice for 30 min and then centrifuged at 13,000 rpm for 15 min at 4 °C.  
433 Supernatant was retained and boiled with 4X SDS loading buffer at 95 °C for 10 min. The denatured  
434 protein samples were separated by 10 % or 12% SDS-PAGE gels and transferred to PVDF membranes  
435 (Millipore). These membranes were blocked with 5% skim milk for 1 h at room temperature and  
436 incubated with the specific primary antibodies at 4 °C overnight. After being washed by TBS-T for 30  
437 min, the membranes were incubated with appropriate HRP-conjugated secondary antibodies at room

438 temperature for 1 h. The bands were visualized by the Automatic Chemiluminescence/Fluorescence  
439 Imaging System (Tanon 5200).

440 **Interferon  $\beta$ -luciferase reporter assay**

441 HEK293T cells (seeded in 96-well plates) were transfected with IFN- $\beta$ -luciferase (50 ng/well), human  
442 STING (50 ng/well) plasmids, different doses of human PCSK9 plasmid (1.5, 2.5, 5 ng/well) or human  
443 SURF4 plasmid (10, 20, 40 ng) for 12 h. The HEK293T cells were stimulated with 0.5  $\mu$ M cGAMP in  
444 the presence of 0.02 mg/mL PFO for another 12 h. Alternatively, HEK293T cells were transfected with  
445 IFN- $\beta$ -luciferase (50 ng/well), human cGAS (30 ng/well), and STING (50 ng/well) plasmids with vector  
446 (20 ng), PCSK9 (5 ng or 20 ng), and SURF4 (20 ng) for 24 h. The IFN- $\beta$  reporter activity was detected  
447 according to the standard protocol.

448 **Immunofluorescence microscopy**

449 For immunofluorescence staining, HeLa cells stably expressing STING-110-GFP or STING-GFP were  
450 cultured on coverslips in 24-well plates and treated as described in the figure legends. After removing  
451 the medium, cells were fixed with 4% paraformaldehyde (Solarbio) for 10 min at room temperature and  
452 then washed with PBS three times. Cells were blocked by staining buffer containing 3% BSA and 0.05%  
453 Triton X-100 for 1 h and then incubated with specific primary antibodies overnight at 4° C. After  
454 washing three to four times in PBS, cells were incubated with secondary antibodies conjugated to Alexa  
455 Fluor 488 or 568 (Invitrogen) and 4',6-diamidino-2-phenylindole (DAPI) for nuclear staining for 2 h at  
456 room temperature. The confocal images were acquired with a Zeiss LSM980 laser scanning microscope.  
457 Zen Blue 3.2 software and Image J software were used for image processing.

458 **Co-Immunoprecipitation of SURF4**

459 BMDCs were seeded at  $3 \times 10^6$  cells/well in 6-well plates. After overnight culture, BMDCs were  
460 pretreated with 20  $\mu$ g/ml siRNA siPCSK9 or siCtrl for 24 h and then treated with 400  $\mu$ M Mn<sup>2+</sup> for 3 h.  
461 SURF4 Co-IP samples were prepared by Pierce™ Direct Magnetic IP/Co-IP Kit (Thermofisher, Cat#  
462 88828) following previously reported methods with slight modifications<sup>34</sup>. Briefly, cells were lysed by  
463 IP buffer in IP/Co-IP Kits supplemented with 1% 3-[3-Cholamidopropyl] dimethylammonio]-1-

464 propanesulfonate (CHAPS), and beads were washed by wash buffer IP/Co-IP Kits supplemented with  
465 0.7% CHAPS (MCE, Cat# HY-15435 ) for stabilized protein-protein complexes and retained the  
466 biochemical activity of proteins in solution.

467 **Protein-protein molecular docking and molecular dynamics simulation**

468 The molecular docking assays of human PCSK9 (PDB id:6U2F) and human STING (PDB id:6NT5)  
469 with human SURF4 (AlphaFold:AF-B7Z1G8-F1) were performed by HDOCK, and the top three  
470 structures with the best docking scores were chosen for subsequent molecular dynamic (MD) simulation.  
471 The protein–protein complex was placed in a cubic box filled with solvent (TIP3P water molecules), and  
472 the complex was simulated by Gromacs 2022.1 under constant temperature (310K, V-rescale  
473 temperature coupling method), pressure (1 bar, Berendsen method), and Charmm36 force field for 50 ns  
474 MD simulation and finally visualized by Pymol.  
475 MM-PBSA (Molecular Mechanics Poisson Boltzmann Surface Area) methods were used to calculate the  
476 binding free energy of the docked complexes between PCSK9/STING and SURF4. A stable segment of  
477 the RMSD (Root mean square deviation) was selected as a frame for PCSK9 (11.5 ns to 37.5 ns) and  
478 STING (6.5 ns to 32.5 ns) for the MM-PBSA estimation. As SURF4 is a membrane protein, the  
479 membrane protein parameters were used for the free energy calculation in this system. The membrane  
480 center position was set as T36, the upper side of the membrane was L25, and the lower side was F46.

481 **Cryogenic Electron Microscopy (Cryo-EM)**

482 Copper carbon grids (Quantifoil R 1.2/1.3, 300 mesh) were pre-treated with a 30-second glow discharge  
483 at a medium level using a Harrick plasma cleaner (PDC-32G-2). Liposome samples were applied to the  
484 grids in a Vitrobot Mark IV (Thermo Fisher) under conditions of 100% humidity and 8°C. After a 10-  
485 second equilibration, an excess sample was blotted on both sides of the grid using filter paper with a blot  
486 force of -1 to 1 for 3.5 seconds. The grids were then vitrified by plunging into liquid ethane and  
487 subsequently stored in a liquid nitrogen-cooled container until further evaluation. Grid quality was  
488 assessed using a Talos Arctica 200 kV electron microscope equipped with a K2 camera (Gatan).

489 **Animal studies**

490 The mice used in this research include C57BL/6 mice (6–8 weeks, purchased from Laboratory Animal  
491 Resources Center of Tsinghua University), CB-17 SCID mice (6 weeks, purchased from Vital River,  
492 China), and BALB/c mice (6–8 weeks, purchased from Vital River, China). All animals were housed  
493 under controlled conditions (constant temperature:  $22 \pm 2^\circ\text{C}$ ; constant humidity:  $50 \pm 10\%$ ; 12 h  
494 dark/light cycle). To evaluate the tissue distribution of indicated formulations, tumor-bearing mice were  
495 intravenously injected with the NP<sup>siPCSK9/Mn<sup>2+</sup></sup>, NP<sup>siPCSK9</sup>, or NP<sup>Mn<sup>2+</sup></sup> (labeled by DiR, 20 µg/ml, MCE,  
496 Cat# HY-D1048) on day 3 post inoculation of  $3 \times 10^5$  tumor cells in the right flank of C57BL/6 mice. The  
497 mice were monitored using the IVIS Spectrum 3D system (Caliper Life Sciences) at 0, 1, 6, 24, 48, and  
498 72 h after intravenous injection. After whole body imaging at the last time point, animals were  
499 euthanized, and the DiR fluorescence signals in the heart, liver, spleen, lung, kidney, and tumor were  
500 imaged by the IVIS Spectrum 3D system (Caliper Life Sciences).

501 To evaluate the therapeutic efficacy of siPCSK9 and STING agonist-containing NP with right flank  
502 MC38 tumors, female C57BL/6 mice of age 6–8 weeks or female C57BL/6<sup>STING<sup>-/-</sup></sup> mice  
503 (GemPharmatech) of age 6–8 weeks were subcutaneously inoculated with  $3 \times 10^5$  MC38 cells on the right  
504 flank on day 0. Tumor-bearing mice were intravenously injected with NP<sup>siPCSK9/Mn<sup>2+</sup></sup>, NP<sup>siPCSK9</sup>, or  
505 NP<sup>Mn<sup>2+</sup></sup> (containing 100 µg/dose siPCSK9 and/or 40 µg/dose Mn<sup>2+</sup>), or intravenously injected with the  
506 control formulation NP<sup>siPCSK9/Mn<sup>2+</sup></sup> (containing 100 µg/dose siCtrl and 40 µg/dose Mn<sup>2+</sup>) on days 8, 11,  
507 and 14. In some experiments, animals were treated with NP<sup>siPCSK9/cGAMP</sup>, NP<sup>siPCSK9</sup>, or NP<sup>cGAMP</sup>  
508 (containing 100 µg/dose siPCSK9 and/or 1.5 µg/dose cGAMP) on day 8. Tumor size was monitored  
509 every 3 days, and tumor volume was calculated by the following equation: tumor volume =  
510 length × width<sup>2</sup> × 0.5.

511 To evaluate the safety of siPCSK9 and STING agonist-containing, MC38 tumor-bearing mice were  
512 intravenously injected with indicated formulations NP<sup>Blank</sup>, NP<sup>siPCSK9</sup>, NP<sup>Mn<sup>2+</sup></sup>, or NP<sup>siPCSK9/Mn<sup>2+</sup></sup> on day 8,  
513 and serum samples were collected at 24, 48, and 96 h post injection. Serum aspartate transaminase  
514 (AST), alanine aminotransferase (ALT), creatinine (CR), and creatine kinase (CK) levels were detected  
515 by an automatic clinical chemistry analyzer (Rayto Chemary-800). Plasma cytokines (IL-6, IFN-β, and

516 TNF $\alpha$ ) were detected by mouse IL-6 ELISA Kit (Cat# GEM0001), mouse IFN-beta ELISA Kit (Cat#  
517 GEM0018), and mouse TNF-alpha ELISA Kit (Cat# GEM0004), respectively. Animals were  
518 euthanized, and major organs such as the heart, liver, spleen, lung, and kidney were collected at 72 h for  
519 H&E staining.

520 For studies with right flank B16F10 tumors, female C57BL/6 mice of age 6–8 weeks (From the  
521 Laboratory Animal Resources Center of Tsinghua University) were subcutaneously inoculated with  
522  $2 \times 10^5$  B16F10 tumor cells on the right flank on day 0. When tumor volumes reached approximately 50  
523 mm<sup>3</sup> (day 6), mice were intravenously administered with NP<sup>cGAMP</sup> (containing 5  $\mu$ g/dose cGAMP) or  
524 NP<sup>siPCSK9/cGAMP</sup> (containing 100  $\mu$ g/dose siPCSK9 and 1.5  $\mu$ g/dose cGAMP). In some experiments,  
525 animals receiving NP<sup>siPCSK9/cGAMP</sup> on day 7 were intraperitoneally injected with 200  $\mu$ g/dose anti-mouse  
526 PD-L1 antibody (10F.9G2, Selleck, Cat# A2115) on days 6, 9, 12, and 15. Body weight was recorded on  
527 days 9, 10, and 11, and subsequently every 3 days thereafter. Tumor size was measured every 3 days to  
528 evaluate tumor progression.

529 For studies using the xenograft model, CB-17 SCID mice were subcutaneously inoculated with  $1 \times 10^6$   
530 MDA-MB-231 cells on day 0. On day 8, the mice were intravenously administered with a single dose of  
531 NP<sup>siPCSK9/cGAMP</sup> (containing 100  $\mu$ g/dose siPCSK9 and 1.5  $\mu$ g/dose cGAMP) or NP<sup>cGAMP</sup> (containing 5  
532  $\mu$ g/dose cGAMP), along with the indicated formulations. Mice were monitored for tumor growth and  
533 body weight throughout the study. Body weight was recorded on days 9, 10, and 11, and subsequently  
534 every 3 days thereafter. Tumor size was measured every 2-3 days to evaluate tumor progression.

535 For the evaluation of the safety and efficacy of NP<sup>siPCSK9/cGAMP</sup>,  $3 \times 10^5$  MC38 cells were subcutaneously  
536 inoculated into C57BL/6J mice. On day 8, the mice were intravenously administered with a single dose  
537 of NP<sup>siPCSK9/cGAMP</sup> (containing 100  $\mu$ g/dose siPCSK9 and 1.5  $\mu$ g/dose cGAMP) and various doses of  
538 NP<sup>cGAMP</sup> (containing 1.5, 2.5, and 5  $\mu$ g/dose cGAMP), along with the indicated formulations. Mice were  
539 monitored for tumor growth and body weight throughout the study. Body weight was recorded on days  
540 9, 10, and 11, and subsequently every 3 days thereafter. Tumor size was measured regularly to assess  
541 tumor progression. The liver, spleen, tumor, and serum were collected at 0, 12, 24, 48, and 72 hours

542 post-treatment for IFN- $\beta$  detection. Additionally, the liver, spleen, and tumor tissues were collected at 24  
543 hours post-treatment for Western blot analysis, MSB staining, and H&E staining.

544 To examine the *in vivo* antitumor immune responses,  $5 \times 10^5$  MC38 cells were inoculated into C57BL/6J  
545 mice. When the tumor size reached  $\sim 150$  mm $^3$ , NP<sup>SiPCSK9/cGAMP</sup>, NP<sup>SiPCSK9</sup>, or NP<sup>cGAMP</sup> (containing 100  
546  $\mu\text{g}/\text{dose}$  siPCSK9 and/or 1.5  $\mu\text{g}/\text{dose}$  cGAMP) were intravenously injected into the mice. Tumor tissues  
547 were harvested on the indicated days and cut into small pieces, followed by dissociation using the  
548 digestion buffer (1 mg/ml collagenase and 100  $\mu\text{g}/\text{ml}$  deoxyribonuclease I in serum-free RPMI) for 30 min  
549 at 37°C with gentle shaking. The obtained suspension was passed through a 70- $\mu\text{m}$  cell strainer to obtain  
550 the single-cell suspension. For surface marker staining, the cells were incubated with anti-mouse CD16/32  
551 (92, Biolegend, Cat# 101302) for 10 min at room temperature, and then incubated with PerCP anti-mouse  
552 CD45 (30-F11, Biolegend, Cat# 103130), APC anti-mouse CD11c (N418, Biolegend, Cat# 117310),  
553 APC/Cy7 anti-mouse F4/80 (BM8, Biolegend, Cat# 123118), FITC anti-mouse CD80 (16-10A1,  
554 Biolegend, Cat# 104706), PE/Cy7 anti-mouse CD86 (GL-1, Biolegend, Cat# 105014), PE anti-mouse  
555 CD206 (MMR) (C068C2, Biolegend, Cat# 141706), FITC anti-mouse CD3 (17A2, Biolegend, Cat#  
556 100204), APC/Cy7 anti-mouse CD4 (GK1.5, Biolegend, Cat# 100414), PE anti-mouse CD8 $\alpha$  (53-6.7,  
557 Biolegend, Cat# 100708), FITC anti-mouse CD45 (30-F11, Biolegend, Cat# 103108), PE/Cy7 anti-mouse  
558 NK-1.1 (PK136, Biolegend, Cat# 108714), BV605-anti-mouse CD69 (H1.2F3, Biolegend, Cat# 104530),  
559 APC anti-mouse/human CD11b (M1/70, Biolegend, Cat# 101212), PE anti-mouse Ly-6G/Ly-6C (Gr-1)  
560 (RB6-8C5, Biolegend, Cat# 108408), PE anti-mouse CD3 (17A2, Biolegend, Cat# 100206) and PerCP  
561 anti-mouse CD25 (PC61, Biolegend, Cat# 102028) at 4°C for 1 h. For intracellular marker staining, the  
562 single-cell suspension was fixed and permeabilized using the Foxp3/Transcription Factor  
563 Fixation/Permeabilization kit (eBioscience), and then stained with PE anti-mouse FOXP3 antibody (MF-  
564 14, Biolegend, Cat# 126404) at 4°C for 1 h. Cells were washed twice before flow cytometry analysis (BD  
565 LSRIFortessa SORP). Data were collected using BD FACSDiva Software v8.0 and analyzed using BD  
566 FlowJo™ Software (v10.6.2).

567 To investigate which population of immune cells contributed to the therapeutic efficacy of  
568 NP<sup>siPCSK9/cGAMP</sup>, 200 µg/dose anti-mouse CD4 (GK1.5, Selleck, Cat# A2101), anti-mouse CD8α (2.43,  
569 Selleck, Cat# A2102), anti-mouse NK1.1 (PK136, Selleck, Cat# A2114) and clodronate liposomes  
570 (LIPOSOMA, Cat# C-005) were intraperitoneally injected into MC38 tumor-bearing mice on day -1, 1,  
571 3, 5, 7 post the first injection of NP<sup>siPCSK9/cGAMP</sup> (2 injections in total at 3-day intervals) to specifically  
572 deplete endogenous CD4<sup>+</sup> T cells, CD8<sup>+</sup> T cells, NK cells, and macrophages, respectively. Batf3<sup>-/-</sup> mice  
573 were used to test the contribution of cDC1s in the therapeutic effect of NP<sup>siPCSK9/cGAMP</sup>. Rat IgG2b (LTF-  
574 2, Selleck, Cat# A2116) was used as the isotype control for those *in vivo* depleting antibodies.

575 To measure antigen presentation on dendritic cells, female C57BL/6 mice of age 6–8 weeks (Vital  
576 River) were subcutaneously inoculated with  $1.5 \times 10^6$  MC38-OVA tumor cells on the right flank on day 0.  
577 On day 10, tumor-bearing mice were intravenously injected with the indicated formulations. On day 12,  
578 tumor tissues were harvested and cut into small pieces, followed by dissociation using a digestion buffer  
579 (1mg/ml collagenase and 100 µg/ml deoxyribonuclease I in serum-free RPMI) for 30 min at 37°C with  
580 gentle shaking. The obtained suspension was passed through a 70-µm strainer to obtain the single-cell  
581 suspension. Then the cells were incubated with anti-CD45 (30-F11), anti-CD11c (N418), and anti-mouse  
582 SIINFEKL/H-2K<sup>b</sup> antibody (25-D1.16) on ice for 20 min before flow cytometry (BD LSRII Fortessa  
583 SORP). Flow cytometric data were collected using BD FACSDiva Software v8.0. The frequency of  
584 antigen-specific CD8α<sup>+</sup> T cells in the tumor was analyzed following previously reported protocols.  
585 Briefly, female C57BL/6 mice of age 6–8 weeks (Vital River) were subcutaneously inoculated with  
586  $1.5 \times 10^6$  MC38-OVA tumor cells on the right flank on day 0. On day 10, tumor-bearing mice were  
587 intravenously injected with the indicated formulations. On day 16, animals were euthanized, and tumors  
588 were harvested and prepared into single-cell suspensions as described above. The cells were incubated  
589 with CD16/32 (1:20) for 10 min and then incubated with peptide-MHC tetramer (H-2K<sup>b</sup>-restricted  
590 SIINFEKL) for 30 min at room temperature and stained with anti-CD45 (30-F11), anti-CD3 (17A2), and  
591 anti-CD8α (53-6.7) on ice for 20 min. Cells were washed twice with FACS buffer and resuspended in  
592 DAPI before flow cytometry.

593 **Statistical analysis**

594 All quantitative data are presented as mean  $\pm$  standard deviation (SD). Statistical analyses were  
595 performed using one-way analysis of variance (ANOVA) followed by Tukey's multiple comparisons  
596 post hoc test, unless otherwise specified. The n number indicates the number of independent  
597 experiments, animals, or cell samples, as defined in each figure legend. For all representative images  
598 (e.g., immunofluorescence or blots), the number of independent experiments with similar results is  
599 indicated in the legend. Assumptions of normality and homogeneity of variance were confirmed prior to  
600 statistical analysis. Exact p-values are provided in the figures, legends, or Source Data file. Independent  
601 experiments rather than technical replicates were used for all statistical analyses unless otherwise stated.

602 **Reporting summary**

603 Further information on research design is available in the Nature Portfolio Reporting Summary linked to  
604 this article.

605 **Data Availability**

606 The authors declare that data supporting the findings of this study are available within the article,  
607 Supplementary, or Source data files. RNA sequencing datasets have been deposited to the NCBI-  
608 Sequence Read Archive (SRA) under accession code SRP607162. The link of this project is  
609 <https://www.ncbi.nlm.nih.gov/sra/PRJNA1301533>. Source data are provided with this paper.

610 **Code Availability**

611 Protein structure predictions in this study were generated using AlphaFold2, which was run locally with  
612 standard structure databases and is freely accessible for non-commercial use (<https://alphafold.ebi.ac.uk/>  
613 ). For protein complex modeling, predictions were performed using AlphaFold3 via the on-demand  
614 server(<https://deepmind.google/science/alphafold/alphafold-server/>).

615 **References**

- 616 1 Demaria, O. *et al.* Harnessing innate immunity in cancer therapy. *Nature* **574**, 45-56 (2019).  
617 <https://doi.org/10.1038/s41586-019-1593-5>
- 618 2 Samson, N. & Ablasser, A. The cGAS-STING pathway and cancer. *Nat Cancer* **3**, 1452-1463  
619 (2022). <https://doi.org/10.1038/s43018-022-00468-w>
- 620 3 Cao, L. L. & Kagan, J. C. Targeting innate immune pathways for cancer immunotherapy.  
621 *Immunity* **56**, 2206-2217 (2023). <https://doi.org/10.1016/j.jimmuni.2023.07.018>
- 622 4 Chen, Q., Sun, L. J. & Chen, Z. J. J. Regulation and function of the cGAS-STING pathway of  
623 cytosolic DNA sensing. *Nature Immunology* **17**, 1142-1149 (2016).  
<https://doi.org/10.1038/ni.3558>
- 625 5 Chin, E. N., Sulpizio, A. & Lairson, L. L. Targeting STING to promote antitumor immunity.  
626 *Trends in Cell Biology* **33**, 189-203 (2023). <https://doi.org/10.1016/j.tcb.2022.06.010>
- 627 6 Deng, L. F. *et al.* STING-Dependent Cytosolic DNA Sensing Promotes Radiation-Induced Type  
628 I Interferon-Dependent Antitumor Immunity in Immunogenic Tumors. *Immunity* **41**, 843-852  
629 (2014). <https://doi.org/10.1016/j.jimmuni.2014.10.019>
- 630 7 Woo, S. R. *et al.* STING-Dependent Cytosolic DNA Sensing Mediates Innate Immune  
631 Recognition of Immunogenic Tumors (vol 41, pg 830, 2014). *Immunity* **42**, 199-199 (2015).  
<https://doi.org/10.1016/j.jimmuni.2014.12.015>
- 633 8 Ishikawa, H., Ma, Z. & Barber, G. N. STING regulates intracellular DNA-mediated, type I  
634 interferon-dependent innate immunity. *Nature* **461**, 788-792 (2009).  
<https://doi.org/10.1038/nature08476>
- 636 9 Chin, E. N. *et al.* Antitumor activity of a systemic STING-activating non-nucleotide cGAMP  
637 mimetic. *Science* **369**, 993-999 (2020). <https://doi.org/10.1126/science.abb4255>
- 638 10 Pan, B. S. *et al.* An orally available non-nucleotide STING agonist with antitumor activity.  
639 *Science* **369** (2020). <https://doi.org/10.1126/science.aba6098>
- 640 11 Yu, J. *et al.* Single-Dose Physically Cross-Linked Hyaluronic Acid and Lipid Hybrid  
641 Nanoparticles Containing Cyclic Guanosine Monophosphate-Adenosine Monophosphate  
642 Eliminate Established Tumors. *ACS Nano* **18**, 29942-29955 (2024).  
<https://doi.org/10.1021/acsnano.4c10673>
- 644 12 Aval, L. M., Pease, J. E., Sharma, R. & Pinato, D. J. Challenges and Opportunities in the Clinical  
645 Development of STING Agonists for Cancer Immunotherapy. *J Clin Med* **9** (2020).  
<https://doi.org/ARTN 3323>
- 648 13 Meric-Bernstam, F. *et al.* Phase Ib study of MIW815 (ADU-S100) in combination with  
649 spartalizumab (PDR001) in patients (pts) with advanced/metastatic solid tumors or lymphomas. *J*  
650 *Clin Oncol* **37** (2019). [https://doi.org/DOI 10.1200/JCO.2019.37.15\\_suppl.2507](https://doi.org/DOI 10.1200/JCO.2019.37.15_suppl.2507)
- 651 14 Dane, E. L. *et al.* STING agonist delivery by tumour-penetrating PEG-lipid nanodiscs primes  
652 robust anticancer immunity. *Nat Mater* **21**, 710-720 (2022). <https://doi.org/10.1038/s41563-022-01251-z>

- 654 15 York, A. G. *et al.* Limiting Cholesterol Biosynthetic Flux Spontaneously Engages Type I IFN  
 655 Signaling. *Cell* **163**, 1716-1729 (2015). <https://doi.org/10.1016/j.cell.2015.11.045>
- 656 16 Frank-Kamenetsky, M. *et al.* Therapeutic RNAi targeting PCSK9 acutely lowers plasma  
 657 cholesterol in rodents and LDL cholesterol in nonhuman primates. *Proc Natl Acad Sci U S A*  
 658 **105**, 11915-11920 (2008). <https://doi.org/10.1073/pnas.0805434105>
- 659 17 Lancellotti, P. & Oury, C. A Highly Durable RNAi Therapeutic Inhibitor of PCSK9. *N Engl J*  
 660 *Med* **376**, e38 (2017). <https://doi.org/10.1056/NEJMc1703361>
- 661 18 Wong, C. C. *et al.* The cholesterol uptake regulator PCSK9 promotes and is a therapeutic target  
 662 in APC/KRAS-mutant colorectal cancer. *Nat Commun* **13**, 3971 (2022).  
<https://doi.org/10.1038/s41467-022-31663-z>
- 663 19 Yang, Q. C. *et al.* Targeting PCSK9 reduces cancer cell stemness and enhances antitumor  
 664 immunity in head and neck cancer. *iScience* **26**, 106916 (2023).  
<https://doi.org/10.1016/j.isci.2023.106916>
- 665 20 Sun, C. *et al.* Identification and validation of PCSK9 as a prognostic and immune-related  
 666 influencing factor in tumorigenesis: a pan-cancer analysis. *Front Oncol* **13** (2023).  
<https://doi.org/ARTN 1134063>
- 667 10.3389/fonc.2023.1134063
- 668 21 Bao, X. *et al.* Targeting proprotein convertase subtilisin/kexin type 9 (PCSK9): from bench to  
 669 bedside. *Signal Transduct Target Ther* **9**, 13 (2024). <https://doi.org/10.1038/s41392-023-01690-3>
- 670 22 Snipstad, K., Fenton, C. G., Kjaeve, J., Anderssen, E. & Paulssen, R. New specific molecular  
 671 targets for radiochemotherapy in colorectal cancer. *Febs J* **276**, 121-121 (2009).
- 672 23 Lv, M. Z. *et al.* Manganese is critical for antitumor immune responses via cGAS-STING and  
 673 improves the efficacy of clinical immunotherapy. *Cell Research* **30**, 966-979 (2020).  
<https://doi.org/10.1038/s41422-020-00395-4>
- 674 24 Wang, C. G. *et al.* Manganese Increases the Sensitivity of the cGAS-STING Pathway for  
 675 Double-Stranded DNA and Is Required for the Host Defense against DNA Viruses. *Immunity* **48**,  
 676 675-+ (2018). <https://doi.org/10.1016/j.immuni.2018.03.017>
- 677 25 Wang, H. Z. *et al.* IFN- $\beta$  Production by TLR4-Stimulated Innate Immune Cells Is Negatively  
 678 Regulated by GSK3- $\beta$ . *J Immunol* **181**, 6797-6802 (2008). <https://doi.org/DOI 10.4049/jimmunol.181.10.6797>
- 679 26 Dobbs, N. *et al.* STING Activation by Translocation from the ER Is Associated with Infection  
 680 and Autoinflammatory Disease. *Cell Host Microbe* **18**, 157-168 (2015).  
<https://doi.org/10.1016/j.chom.2015.07.001>
- 681 27 Ogawa, E., Mukai, K., Saito, K., Arai, H. & Taguchi, T. The binding of TBK1 to STING  
 682 requires exocytic membrane traffic from the ER. *Biochem Biophys Res Co* **503**, 138-145 (2018).  
<https://doi.org/10.1016/j.bbrc.2018.05.199>
- 683 28 Jeltema, D., Abbott, K. & Yan, N. STING trafficking as a new dimension of immune signaling. *J*  
 684 *Exp Med* **220** (2023). <https://doi.org/10.1084/jem.20220990>

- 692 29 Srikanth, S. *et al.* The Ca(2+) sensor STIM1 regulates the type I interferon response by retaining  
 693 the signaling adaptor STING at the endoplasmic reticulum. *Nat Immunol* **20**, 152-162 (2019).  
 694 <https://doi.org/10.1038/s41590-018-0287-8>
- 695 30 Ishikawa, H. & Barber, G. N. Sting is an endoplasmic reticulum adaptor that facilitates innate  
 696 immune signaling. *Cytokine* **48**, 128-128 (2009). <https://doi.org/10.1016/j.cyto.2009.07.543>
- 697 31 Hopfner, K. P. & Hornung, V. Molecular mechanisms and cellular functions of cGAS-STING  
 698 signalling. *Nat Rev Mol Cell Biol* **21**, 501-521 (2020). <https://doi.org/10.1038/s41580-020-0244-x>
- 700 32 Deng, Z. *et al.* A defect in COPI-mediated transport of STING causes immune dysregulation in  
 701 COPA syndrome. *J Exp Med* **217** (2020). <https://doi.org/10.1084/jem.20201045>
- 702 33 Lepelley, A. *et al.* Mutations in COPA lead to abnormal trafficking of STING to the Golgi and  
 703 interferon signaling. *J Exp Med* **217** (2020). <https://doi.org/10.1084/jem.20200600>
- 704 34 Mukai, K. *et al.* Homeostatic regulation of STING by retrograde membrane traffic to the ER. *Nat  
 705 Commun* **12**, 61 (2021). <https://doi.org/10.1038/s41467-020-20234-9>
- 706 35 Shen, Y., Gu, H. M., Qin, S. & Zhang, D. W. Surf4, cargo trafficking, lipid metabolism, and  
 707 therapeutic implications. *J Mol Cell Biol* **14** (2023). <https://doi.org/10.1093/jmcb/mjac063>
- 708 36 Yan, R., Chen, K., Wang, B. & Xu, K. SURF4-induced tubular ERGIC selectively expedites ER-  
 709 to-Golgi transport. *Dev Cell* **57**, 512-525 e518 (2022).  
<https://doi.org/10.1016/j.devcel.2021.12.018>
- 710 37 Zanetti, G., Pahuja, K. B., Studer, S., Shim, S. & Schekman, R. COPII and the regulation of  
 712 protein sorting in mammals. *Nat Cell Biol* **14**, 20-28 (2011). <https://doi.org/10.1038/ncb2390>
- 713 38 Emmer, B. T. *et al.* The cargo receptor SURF4 promotes the efficient cellular secretion of  
 714 PCSK9. *eLife* **7** (2018). <https://doi.org/10.7554/eLife.38839>
- 715 39 Brandizzi, F. & Barlowe, C. Organization of the ER-Golgi interface for membrane traffic  
 716 control. *Nat Rev Mol Cell Biol* **14**, 382-392 (2013). <https://doi.org/10.1038/nrm3588>
- 717 40 Zhang, B. C. *et al.* Cholesterol-binding motifs in STING that control endoplasmic reticulum  
 718 retention mediate anti-tumoral activity of cholesterol-lowering compounds. *Nat Commun* **15**,  
 719 2760 (2024). <https://doi.org/10.1038/s41467-024-47046-5>
- 720 41 Luo, Z. J., Dai, Y. & Gao, H. L. Development and application of hyaluronic acid in tumor  
 721 targeting drug delivery. *Acta Pharm Sin B* **9**, 1099-1112 (2019).  
<https://doi.org/10.1016/j.apsb.2019.06.004>
- 723 42 Uhlen, M. *et al.* Towards a knowledge-based Human Protein Atlas. *Nat Biotechnol* **28**, 1248-  
 724 1250 (2010). <https://doi.org/10.1038/nbt1210-1248>
- 725 43 Liu, X. *et al.* Inhibition of PCSK9 potentiates immune checkpoint therapy for cancer. *Nature*  
 726 **588**, 693-698 (2020). <https://doi.org/10.1038/s41586-020-2911-7>

## 727 Acknowledgements

728 The work was supported in part by grants from National Natural Science Foundation of China  
 729 (82173751, 32070875), National Key Research and Development Program of China

730 (2023YFC3403100), National High-Level Young Talent Program, Tsinghua University Initiative  
731 Scientific Research Program (2024Z11DSZ001, 2025Z11DSZ001, 2022Z11QYJ036), start-up packages  
732 from Tsinghua University, support from Tsinghua-Peking Center for Life Sciences, and support from  
733 the Key Laboratory of Innovative Drug Research and Evaluation. We thank Prof. Meng Xu (School of  
734 Medicine, Tsinghua University) for kindly providing the murine colon adenocarcinoma cells (MC38).  
735 We would like to acknowledge Bingyu Liu from the Imaging Core Facility, Technology Center for  
736 Protein Sciences, Tsinghua University, for her assistance with the Zeiss LSM980 laser scanning  
737 microscopy. We would like to acknowledge Weihua Wang at the Center of Pharmaceutical Technology,  
738 Tsinghua University, for her assistance with liquid chromatography-mass spectrometry (LC-MS)  
739 analysis. We would like to acknowledge Xiangjie Ge and Yanjie Li from the Cryo-EM Facility of the  
740 China National Center for Protein Sciences (Beijing), Tsinghua University, for their support on the FEI  
741 Tecnai Arctica TEM D683.

742 **Author contributions**

743 P.S., F.H., C.Z., and R.K. designed the experiments. P.S., F.H., X.L., C.W., T.D., and J.H. performed  
744 the experiments. P.S., F.H., C.Z., and R.K. analyzed the data. All authors have given approval to the  
745 final version of the manuscript.

746 **Competing interests**

747 A patent application (2023107003368) has been filed based on the findings described in the manuscript,  
748 with R.K., P.S., C.Z., and F.H. as inventors. The remaining authors declare no competing interests.  
749

750 **Figure 1. PCSK9 silencing enhances cGAS-STING activation.** (a) Schematic illustrating the aim and  
 751 strategy of the clinical data analysis. b-g, Correlations between PCSK9 and indicated innate immune  
 752 signaling-related genes. Shown are mRNA levels of (b) PCSK9 and IFN- $\beta$ , (c) PCSK9 and ISG20, (d)  
 753 PCSK9 and STING, (e) PCSK9 and MAVS, (f) PCSK9 and IL-6, and (g) PCSK9 and IL-1 $\beta$  (GEO  
 754 dataset: GSE15781, n = 42 patients). h-i, BMDCs were incubated with siPCSK9 (h) or siCtrl (i) and/or  
 755 different concentrations of Mn<sup>2+</sup>. After 24 h, IFN- $\beta$  secretion was quantified by ELISA (n = 3  
 756 independent experiments). j and k, Dose-response curves of the IFN- $\beta$  response in BMDCs after  
 757 siPCSK9 or siCtrl treatment (n = 3 independent experiments). The EC<sub>50</sub> values are shown for the  
 758 indicated formulations. l, Raw264.7 ISG luciferase reporter cells were exposed to Mn<sup>2+</sup> (50  $\mu$ M), and/or  
 759 siPCSK9 (7.5  $\mu$ g/ml) for 24 h before measuring the luciferase signal. m, THP1 ISG luciferase reporter  
 760 cells were exposed to Mn<sup>2+</sup> (50  $\mu$ M), and/or siPCSK9/siCtrl (7.5  $\mu$ g/ml) for 24 h before measuring the  
 761 luciferase signal (n = 3 independent experiments). n, THP1-Luica ISG reporter cells were exposed to c-  
 762 di-AMP (1  $\mu$ M), and/or siPCSK9/siCtrl (7.5  $\mu$ g/ml) for 24 h before measuring the luciferase signal (n = 3  
 763 independent experiments). o, THP1-Lucia ISG reporter cells were exposed to cGAMP (1  $\mu$ M), and/or  
 764 siPCSK9/siCtrl (7.5  $\mu$ g/ml) for 24 h before measuring the luciferase signal (n = 3 independent  
 765 experiments). Data represent mean  $\pm$  SD. Data were analyzed by one-way analysis of variance  
 766 (ANOVA) with Tukey's multiple comparisons post-test (l, m, n, and o) or two-way ANOVA with  
 767 Bonferroni's multiple comparisons post-test (j and k). Source data are provided as a Source Data file.  
 768 Panel (a) was created in BioRender. Kuai, R. (2025) <https://BioRender.com/28bogc8>.

769 **Figure 2. siPCSK9 boosts Type I interferon secretion in a cGAS-STING-dependent manner.** a,  
 770 BMDCs were incubated with siPCSK9 or siCtrl (4  $\mu$ g/well) and/or 10  $\mu$ g/ml Poly (I: C). After 24 h, the  
 771 IFN- $\beta$  secretion was quantified by ELISA (n = 3 independent experiments). b, THP1-Lucia ISG reporter  
 772 cells were exposed to 10  $\mu$ g/ml Poly (I: C) and/or siPCSK9/siCtrl (7.5  $\mu$ g/ml) for 24 h (n = 3  
 773 independent experiments) before measuring the luciferase signal. c, THP1-Lucia ISG reporter cells were  
 774 incubated with siPCSK9 /siCtrl (7.5  $\mu$ g/ml) and/or 10  $\mu$ g/ml Poly (I:C). After 24 h, the IFN- $\beta$  secretion  
 775 was quantified by ELISA (n = 3 independent experiments). d, THP1-Lucia ISG reporter cells were

exposed to 500 ng/ml LPS and/or siPCSK9/siCtrl (7.5  $\mu$ g/ml) for 24 h before measuring the luciferase signal (n = 3 independent experiments). e, THP1-Lucia ISG NF- $\kappa$ B reporter cells were exposed to 500 ng/ml LPS and/or siPCSK9/siCtrl (7.5  $\mu$ g/ml) for 24 h before measuring the luciferase signal (n = 3 independent experiments). f, WT or STING $^{-/-}$  BMDCs were incubated with siPCSK9/siCtrl (4  $\mu$ g/well) and/or Mn $^{2+}$  (400  $\mu$ M). After 24 h, the IFN- $\beta$  secretion was quantified by ELISA (n = 3 independent experiments). g, WT or STING $^{-/-}$  THP1-Lucia ISG reporter cells were exposed to Mn $^{2+}$ (50  $\mu$ M), and/or siPCSK9 /siCtrl (7.5  $\mu$ g/ml) for 24 h before measuring the luciferase signal (n = 3 independent experiments). h-m, Relative expression of (h) *Ifnb*, (i) *Cxcl10*, (j) *Ccl5*, (k) *Isg15*, (l) *Ifit3*, and (m) *Tnfa* mRNA in WT or STING $^{-/-}$  BMDCs treated with siPCSK9/siCtrl (4  $\mu$ g/well) and/or Mn $^{2+}$  (400  $\mu$ M) for 24 h (n = 3 independent experiments). n, Representative confocal images of STING (Green) translocation to Golgi (Red) in WT HeLa-hSTING-GFP or PCSK9-knockout HeLa-hST-GFP (HeLa-hSTING-GFP<sup>PCSK9 KO</sup>) treated with 500  $\mu$ M Mn $^{2+}$  for 3 h (Scale bars 10  $\mu$ m). This experiment was repeated independently three times with similar results. o, Pearson's correlation coefficient of STING and Golgi colocalization of HeLa cells in (n) (n = 50 cells). This experiment was repeated independently three times with similar results. p, Quantification of the number of PCSK9 dots/cell in (q) (n = 50 cells). q, Representative confocal images of STING (Green) translocation and PCSK9 (Red) secretion in HeLa-hSTING-GFP<sup>WT</sup> or HeLa-hSTING-GFP<sup>PCSK9 KO</sup> treated with 500  $\mu$ M Mn $^{2+}$  for 3 h (Scale bar 10  $\mu$ m). r, Representative confocal images of Sec24B (Violet), STING (Green), and PCSK9 (Red) colocalization in HeLa-hSTING-GFP<sup>WT</sup> or HeLa-hSTING-GFP<sup>PCSK9 KO</sup> cells treated with 500  $\mu$ M Mn $^{2+}$  for 3 h (Scale bar 10  $\mu$ m). This experiment was repeated independently three times with similar results. s-t, SURF4, PCSK9, STING, and phosphorylated STING/TBK1 expression in BMDCs treated with siPCSK9/siCtrl (20  $\mu$ g/ml) and/or Mn $^{2+}$  (400  $\mu$ M) for 24 h (s) or in HeLa<sup>WT</sup>/HeLa-hSTING<sup>PCSK9 KO</sup> cells treated with 500  $\mu$ M Mn $^{2+}$  for 12 h (t). This experiment was repeated independently three times with similar results. Data represent mean  $\pm$  SD. NS, not significant. Data were analyzed by one-way analysis of variance (ANOVA) with Tukey's multiple comparisons post-test. In the immunofluorescence images shown in

801 2n, 2q, and 2r, PCSK9 was labeled with fluorescence by using a commercially available antibody, and  
802 STING was tagged with GFP. Source data are provided as a Source Data file.

803 **Figure 3. PCSK9 limits anterograde STING trafficking by competing with the cargo receptor**  
804 **SURF4.** a-d, SURF4, PCSK9, STING, and phosphorylated STING /TBK1/IRF3 expression in THP1<sup>WT</sup>/  
805 THP1<sup>PCSK9 KO</sup>-Lucia ISG reporter cells treated with 50  $\mu$ M Mn<sup>2+</sup>, or in THP1<sup>WT</sup>/THP1<sup>PCSK9 KO</sup> (b),  
806 L929<sup>WT</sup>/ L929<sup>PCSK9 KO</sup> (c), HeLa<sup>WT</sup> / HeLa-hSTING<sup>PCSK9 KO</sup> cells (d), cells treated with 1  $\mu$ M cGAMP  
807 for 0, 2, 4, and 6 h. This experiment was repeated independently three times with similar results. e,  
808 Representative confocal images of STING (Green) translocation in HeLa-hSTING-GFP<sup>WT</sup> or HeLa-  
809 hSTING-GFP<sup>PCSK9 KO</sup> cells treated with 100 nM cGAMP for 0, 1, and 2 h. This experiment was repeated  
810 independently three times with similar results. f, THP1<sup>WT</sup> or THP1<sup>PCSK9 OE</sup>-Lucia reporter cells were  
811 exposed to different concentrations of cGAMP for 24 h (n = 3 independent experiments). g, HEK293T  
812 cells were transfected with STING, different concentrations of PCSK9 plasmid (1.5, 2.5, and 5 ng), and  
813 IFN- $\beta$  promoter-driven luciferase reporter (IFN- $\beta$ -luc) together with or without 0.5  $\mu$ M cGAMP  
814 treatment for 24 h (n = 3 independent experiments). h, HEK293T cells were transfected with cGAS,  
815 STING, SURF4, PCSK9 alone or indicated combinations and IFN- $\beta$  promoter-driven luciferase reporter  
816 (IFN- $\beta$ -luc) together for 24 h (n = 3 independent experiments). i, THP1<sup>WT</sup>, THP1<sup>PCSK9 KO</sup>, or THP1<sup>SURF4</sup>  
817 <sup>OE</sup>-Lucia ISG reporter cells were exposed to 1  $\mu$ M cGAMP for 24 h (n = 3 independent experiments). j,  
818 HEK293T cells were transfected with STING, different concentrations of SURF4 plasmid (10, 20, and  
819 40 ng), and IFN- $\beta$  promoter-driven luciferase reporter (IFN- $\beta$ -luc) together with or without 0.5  $\mu$ M  
820 cGAMP treatment for 24 h (n = 3 independent experiments). k, Co-IP analysis of SURF4 and  
821 PCSK9/STING interactions in lysates from BMDC cells treated with siPCSK9/siCtrl (20  $\mu$ g/ml) and  
822 Mn<sup>2+</sup> alone or indicated combinations for 6 h. This experiment was repeated independently three times  
823 with similar results. l, Co-IP analysis of SURF4 and PCSK9/STING interactions in lysates from  
824 THP1<sup>WT</sup> and THP1<sup>PCSK9 KO</sup> cells treated with cGAMP 1  $\mu$ M for 4 h. This experiment was repeated  
825 independently three times with similar results. Predicted conformation and Gibbs binding energy of  
826 SURF4/PCSK9 complex (m) and SURF4/STING complex (n) via Molecular Dynamics Simulation. (o)

827 Structural clash model of PCSK9 and STING via molecular dynamics simulation. Data represent mean  
828  $\pm$  SD. Data were analyzed by one-way analysis of variance (ANOVA) with Tukey's multiple  
829 comparisons post-test or two-way ANOVA with Bonferroni's multiple comparisons post-test (f). Source  
830 data are provided as a Source Data file.

831 **Figure 4. Engineered nanoparticles co-delivering PCSK9 siRNA and STING agonists for safe and**  
832 **effective cancer immunotherapy.** (a) Schematic showing PCSK9-mediated suppression of STING  
833 activation and the design of bioinspired nanoparticles. (b) Size distribution of NP<sup>siPCSK9/cGAMP</sup> measured  
834 by dynamic light scattering (DLS). This experiment was repeated independently three times with similar  
835 results. (c) Cryo-electron microscopy (cryo-EM) images of NP<sup>siPCSK9/cGAMP</sup>, Scale bar = 50 nm. This  
836 experiment was repeated independently three times with similar results. (d) Heatmap analysis of type I  
837 interferon, MHC I complex, and co-stimulatory signals from RNA sequencing data (n = 3 independent  
838 experiments). (e) C57BL/6 mice were subcutaneously injected with 300,000 MC38 cells on day 0. On  
839 day 8, tumor-bearing mice were intravenously injected with indicated NP formulations containing 100  
840  $\mu$ g/dose siPCSK9 and/or 1.5  $\mu$ g/dose cGAMP (n = 5 mice). Shown are (f) average tumor growth curves,  
841 (g) body weight changes, and (h) tumor growth curves post rechallenge (n = 5 mice). (i-j) C57BL/6 or  
842 C57BL/6<sup>Batf3<sup>-/-</sup></sup> mice were inoculated subcutaneously with  $3 \times 10^5$  MC38 tumor cells on day 0 and  
843 intravenously injected with NP<sup>siPCSK9/cGAMP</sup> on day 8. Average tumor growth curves (i) and survival  
844 curves (j) for animals treated with NP<sup>siPCSK9/cGAMP</sup> and antibodies that deplete indicated populations of  
845 immune cells (n = 5 mice). (k) percentage of CD86<sup>+</sup> cells among CD11C<sup>+</sup> dendritic cells, (l) percentage  
846 of CD8<sup>+</sup> T cells among CD3<sup>+</sup> T cells, (m) M1/M2 macrophage ratio, (n) percentage of CD25<sup>+</sup>Foxp3<sup>+</sup> T  
847 cells among CD4<sup>+</sup> T cells in the tumor microenvironment on day 11 (n = 3 mice).(o) percentage of  
848 SIINFEKL-specific T cells among CD8<sup>+</sup> T cells in the tumor microenvironment on day 11 (n = 3 mice).  
849 Data are presented as mean  $\pm$  SD. Data were analyzed by one-way ANOVA with Tukey's multiple  
850 comparisons test (k, l, m, n, and o). Data were analyzed by two-way ANOVA with Dunnett's multiple  
851 comparisons test (f, g, h, and i). Source data are provided as a Source Data file. Panel (a) was created in  
852 BioRender. Kuai, R. (2025) <https://BioRender.com/b04l005>.

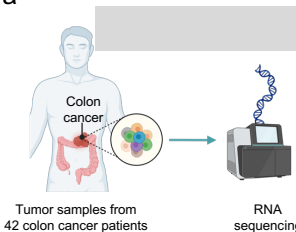
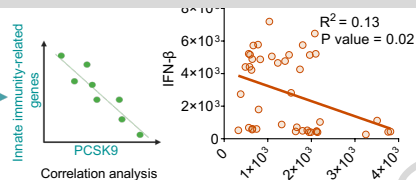
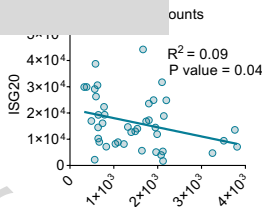
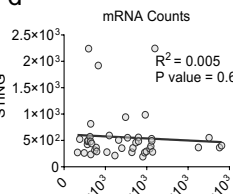
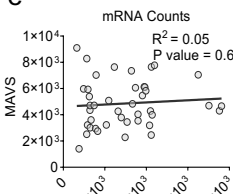
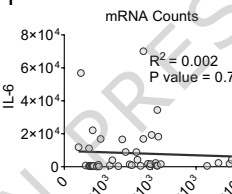
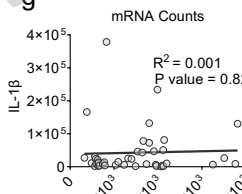
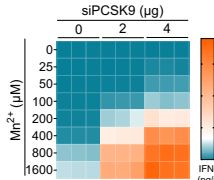
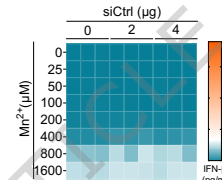
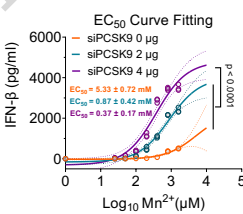
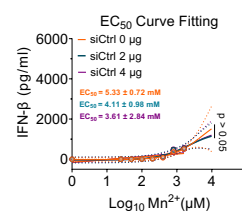
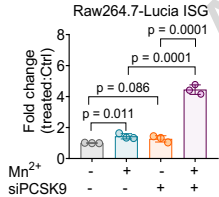
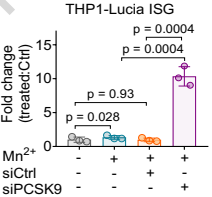
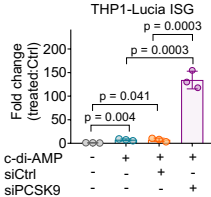
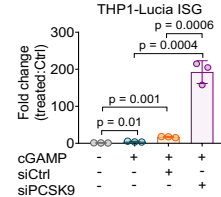
853 **Figure 5. Reshaping the spatiotemporal activation of STING for safe and effective cancer**  
854 **immunotherapy.** (a) Dosing regimen for the treatment of mice bearing MC38 tumors. (b) Average  
855 tumor growth curves and (c) body weight changes of MC38-bearing mice treated with NP formulations  
856 containing 100 µg/dose siPCSK9 and 1.5 µg/dose cGAMP or 1.5, 2.5, 5 µg/dose cGAMP (n = 5 mice).  
857 (d) CB-17 SCID mice were inoculated subcutaneously with  $1 \times 10^6$  MDA-MB-231 tumor cells on day 0  
858 and intravenously treated with the indicated formulations on day 8. (e) Average tumor growth curves for  
859 animals treated with indicated formulations (n = 6 mice). (f) Body weights of animals treated with the  
860 indicated formulations. (g) The survival curves of animals treated with the indicated formulations (n = 6  
861 mice). (h) Representative images of tumor-bearing mice treated with the indicated formulations on days  
862 8 and 21. (i) Individual tumor growth curves for animals treated with indicated formulations (n = 6  
863 mice). (j) C57BL/6 mice were inoculated subcutaneously with  $2 \times 10^5$  B16-F10 tumor cells on day 0,  
864 intraperitoneally injected with αPD-L1 on days 6, 9, 12, and 15, and intravenously injected with the  
865 indicated formulations on day 7. (k) Average tumor growth curves for animals treated with indicated  
866 formulations (n = 6 mice). (l) Body weights of animals treated with indicated formulations. (m) The  
867 survival curves of animals treated with indicated formulations (n = 6 mice). (n) Individual tumor growth  
868 curves for animals treated with indicated formulations (n = 6 mice). (o) Representative images of tumor-  
869 bearing mice treated with indicated formulations on days 6 and 14. Data are presented as mean ± SEM.  
870 Data were analyzed by two-way ANOVA with Dunnett's multiple comparisons test (b, c, e, f, k, and l).  
871 Data were analyzed by log-rank (Mantel–Cox) test (g and m) or two-way analysis of variance  
872 (ANOVA) with Dunnett's multiple comparisons test (c). Source data are provided as a Source Data file.  
873 Panel (a) was created in BioRender. Kuai, R. (2025) <https://BioRender.com/28bogc8>.

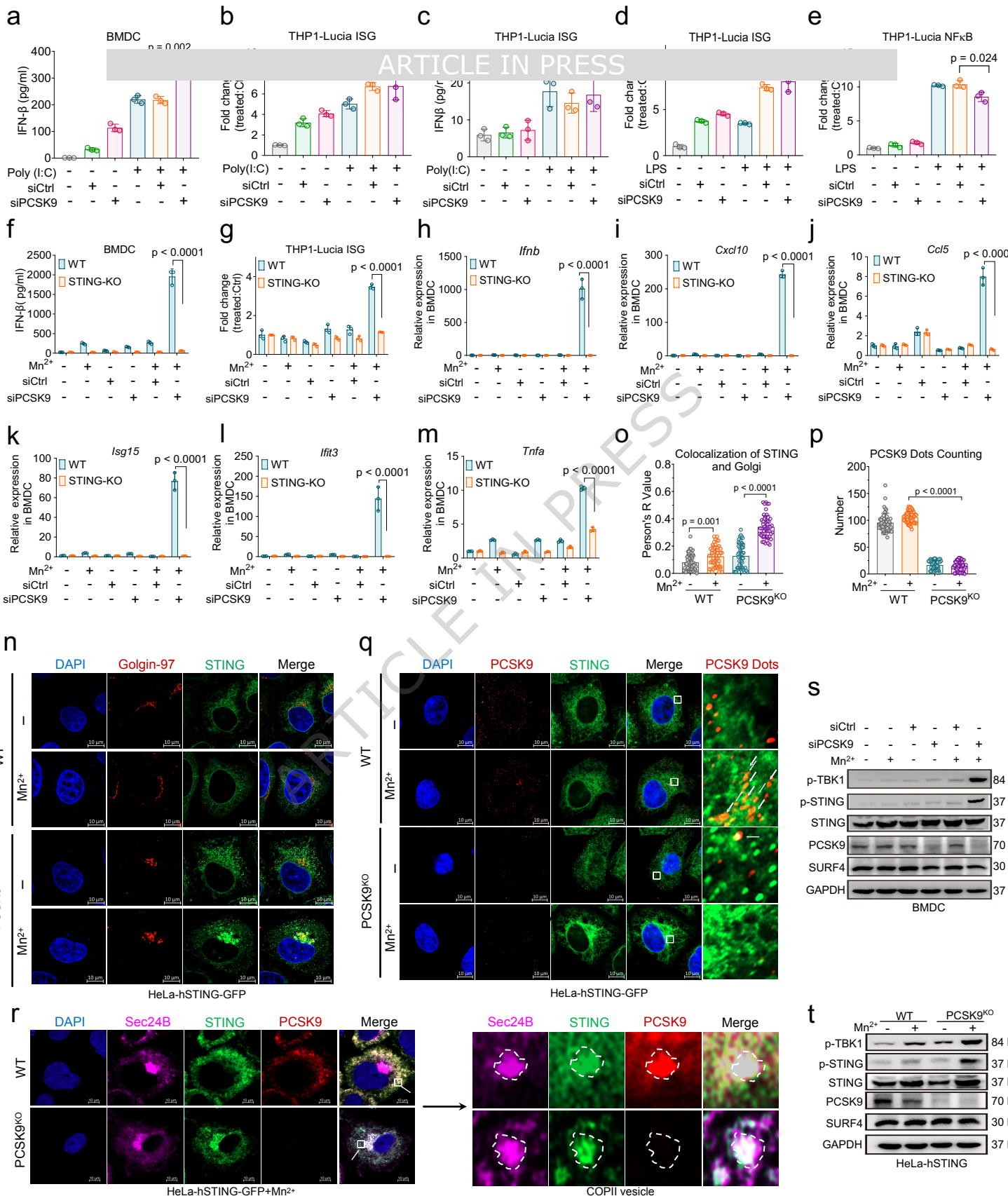
874 **Figure 6. PCSK9 silencing promotes tumor-specific STING activation and spares the liver from**  
875 **toxicity.** (a) STING and PCSK9 expression levels in the liver, spleen, and tumor of untreated mice (n =  
876 3 mice). (b-c) C57BL/6 mice (n = 3 mice) were treated with NP<sup>cGAMP</sup> and NP<sup>siPCSK9/cGAMP</sup> on day 8.  
877 Shown are (e) liver IFN-β levels and (f) serum concentrations of aspartate aminotransferase (AST) at  
878 indicated time points (0, 12, 24, 48, and 72 h post-treatment, n = 3 mice). (d-e) Martius Scarlet Blue

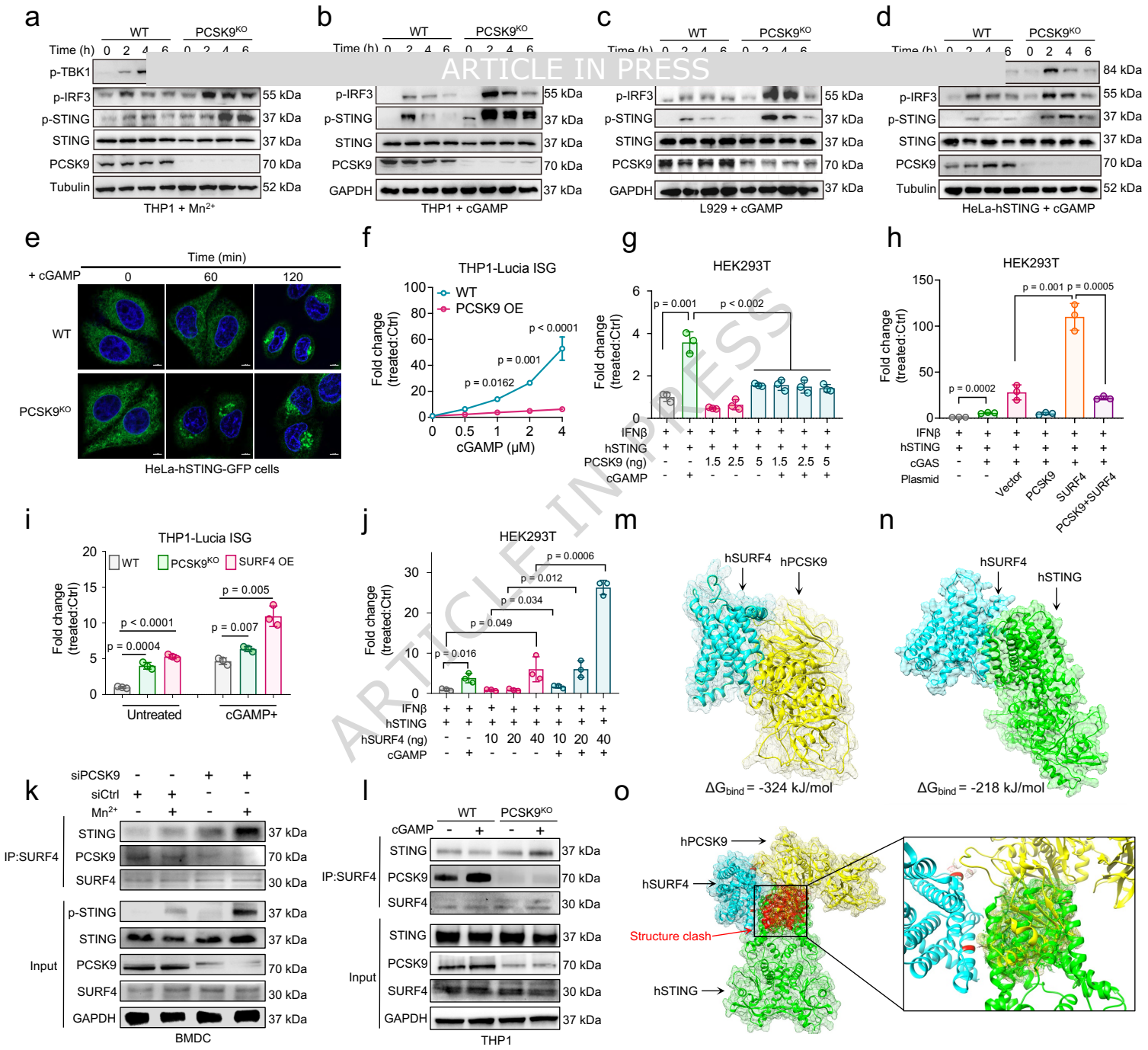
879 (MSB) staining of the liver (d) and tumor (e) after 24 hours of treatment with indicated NP formulations  
880 containing 100 µg/dose siPCSK9 and 1.5 µg/dose cGAMP, or 5 µg/dose cGAMP (n = 3 mice), and  
881 expression of PCSK9 and key proteins related to the STING pathway in the liver (f) and tumor (g). (h)  
882 Schematic showing differential activation patterns of STING in the liver and tumor following systemic  
883 administration of NP<sup>cGAMP</sup> and NP<sup>siPCSK9/cGAMP</sup>. Systemic delivery of NP<sup>cGAMP</sup> (high dose) leads to a lack  
884 of differential STING regulation in the tumor and liver, providing effective cancer immunotherapy but  
885 also causing uncontrollable hepatotoxicity. However, systemic delivery of NP<sup>siPCSK9/cGAMP</sup> induces  
886 differential STING regulation of low-dose cGAMP and siPCSK9 in the tumor and liver, offering the  
887 potential for safe and effective cancer immunotherapy. Data are presented as mean ± SD. AUC data  
888 were calculated from the corresponding curves and subsequently analyzed by one-way ANOVA with  
889 Tukey's multiple comparisons test (b and c). Source data are provided as a Source Data file. Panel (h)  
890 was created in BioRender. Kuai, R. (2025) <https://BioRender.com/obym8jd>.

891 **Figure 7. Evolutionarily conserved structures of SURF4, STING, and PCSK9 across species.**

892 Alphafold2-predicted structures of PCSK9, STING, and SURF4 in Homo sapiens, Pan paniscus, Mus  
893 musculus, Cottoperca gobio, and Ornithorhynchus anatinus, spanning a time range from 300,000 years  
894 to 110 million years.

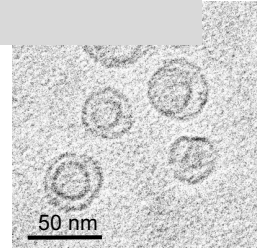
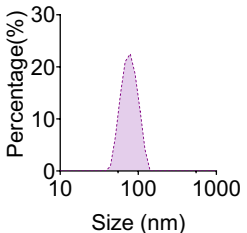
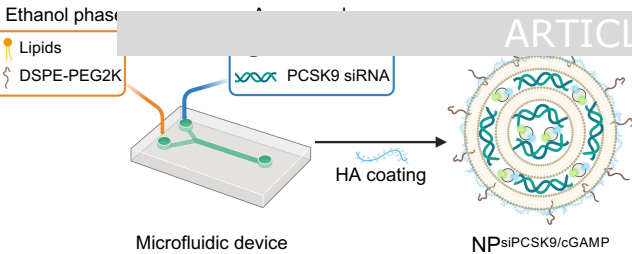
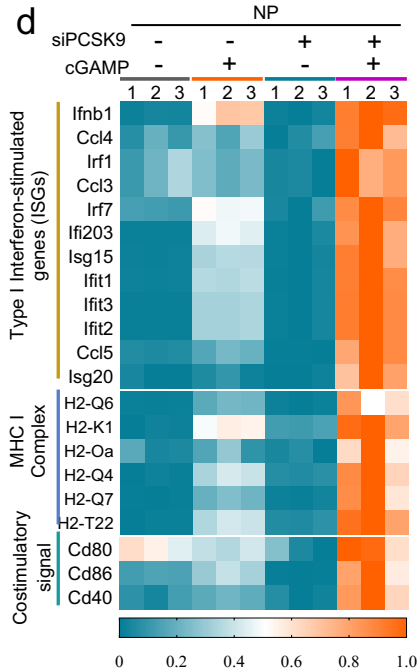
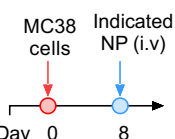
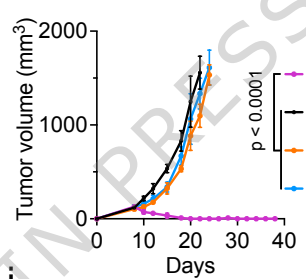
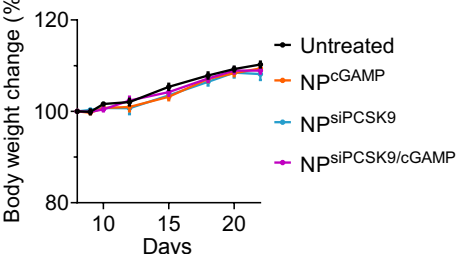
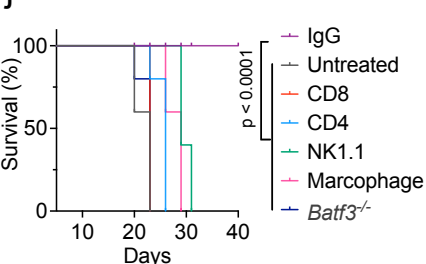
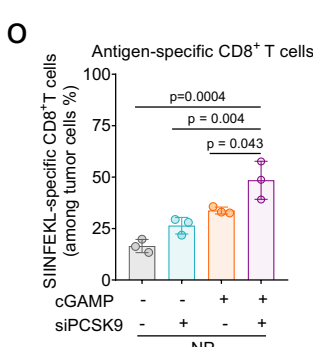
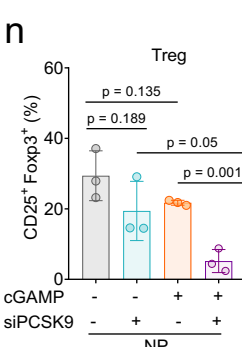
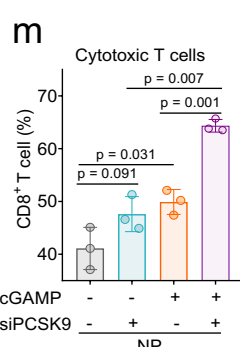
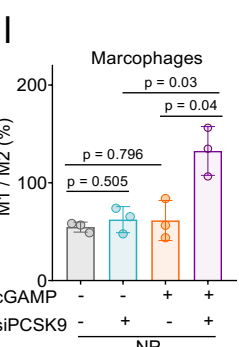
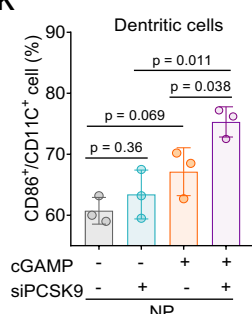
**a****b****c****d****e****f****g****h****i****j****k****l****m****n****o**

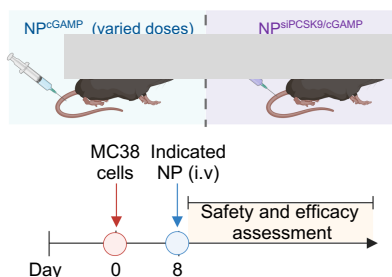
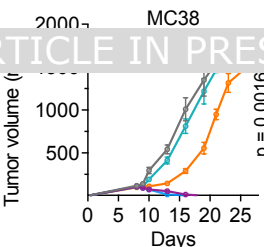
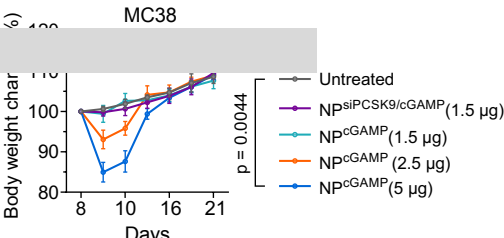
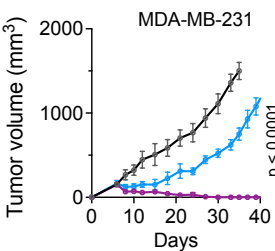
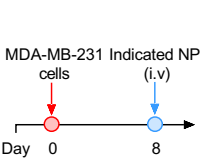
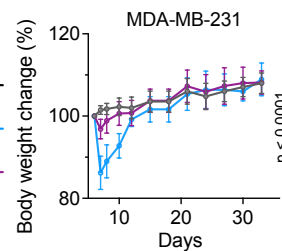
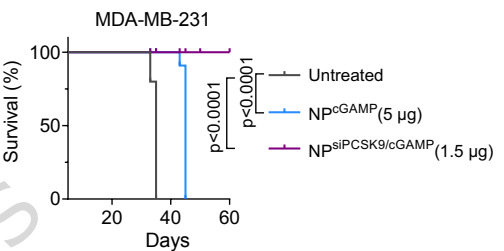
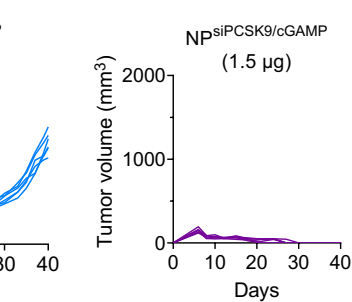
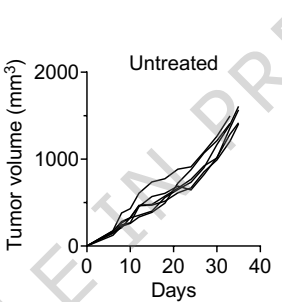
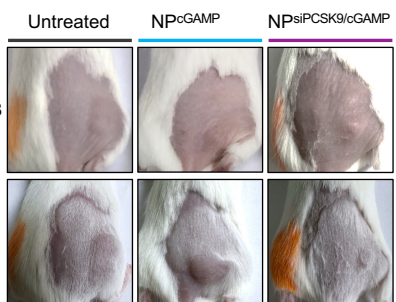
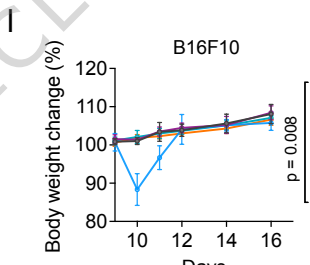
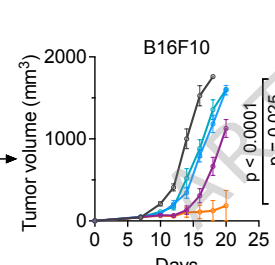
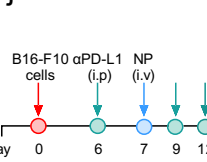
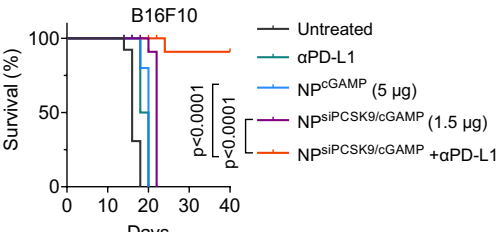
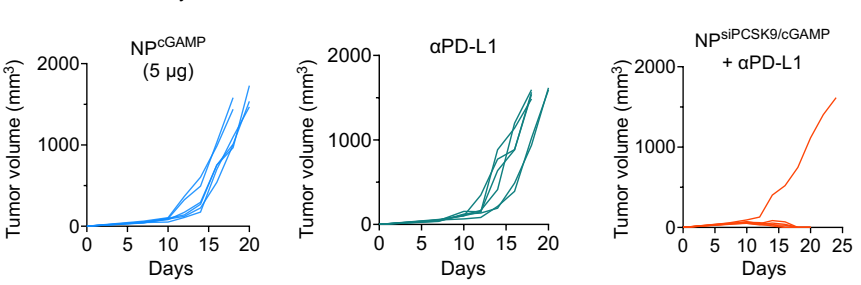
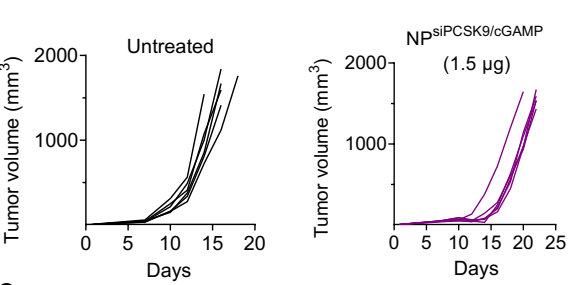
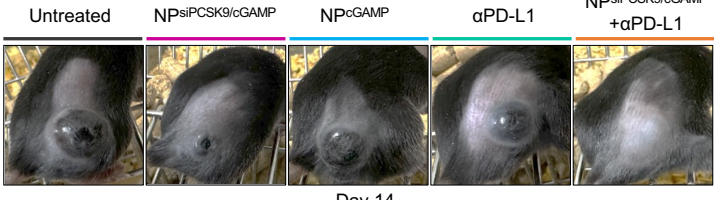
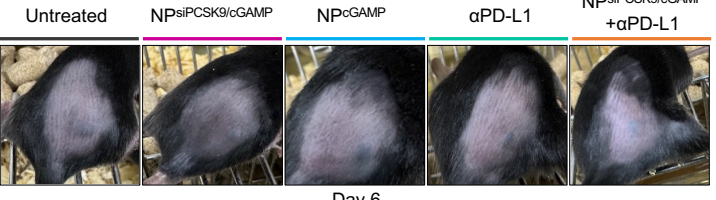




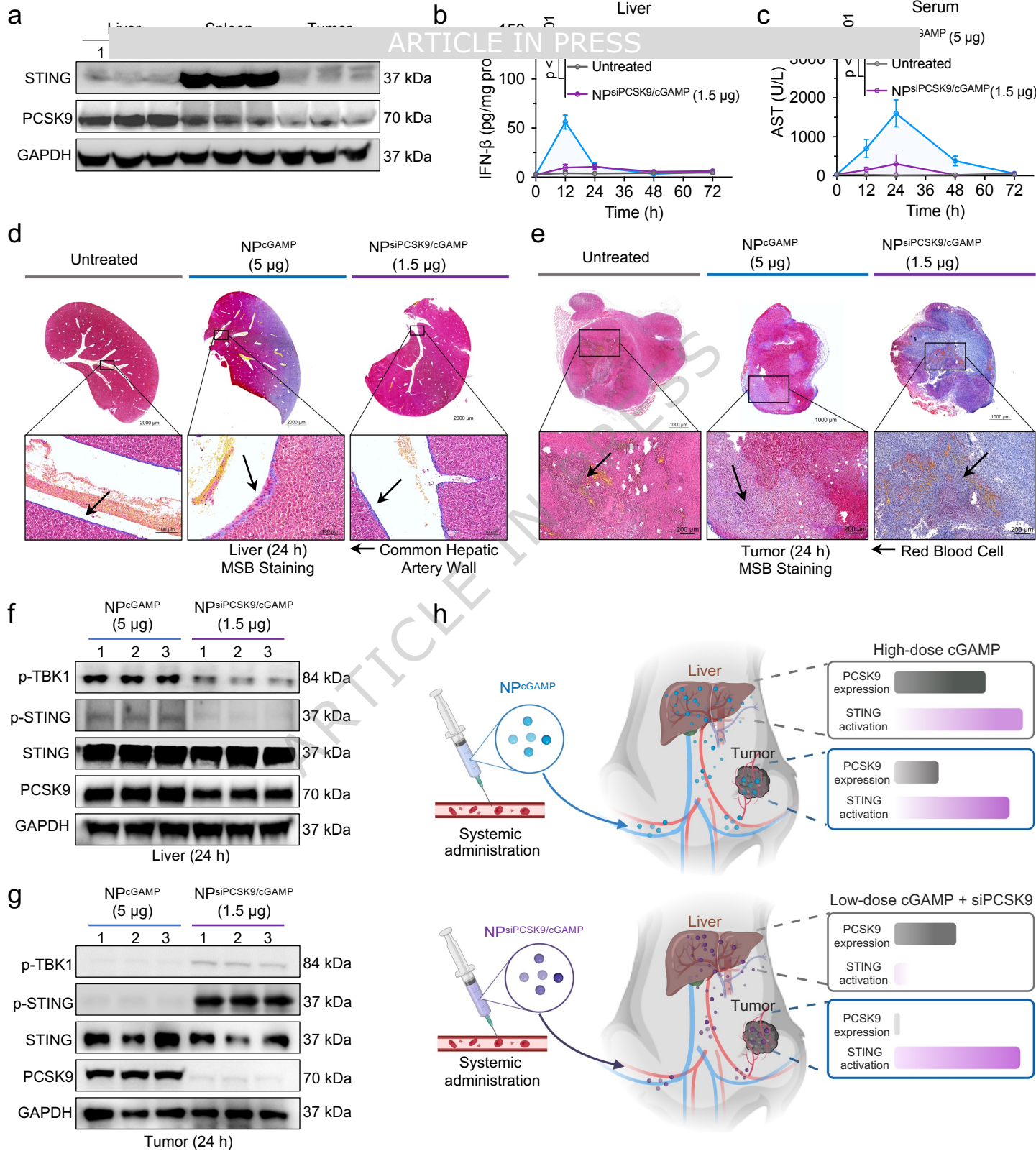
**b**

## ARTICLE IN PRESS

**c**NPs<sub>i</sub>PCSK9/cGAMP**d****e****f****g****j****k**

**a****b****c****d****e****f****h****j****m****n****o**

# ARTICLE IN PRESS



Ancient

Evolutionary history

Modern

110 million years ago 80 million years ago 7 million years ago 0.9 million years ago 200 000 years ago

ARTICLE IN PRESS



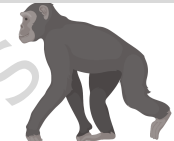
*Ornithorhynchus anatinus*



*Cottoperca gobio*



*Mus musculus*

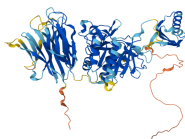


*Pan paniscus*

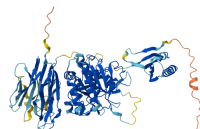


*Homo sapiens*

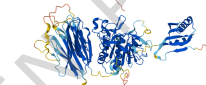
PCSK9



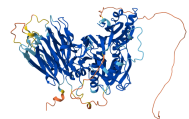
Length (677 aa)



(669 aa)



(696 aa)



(694 aa)

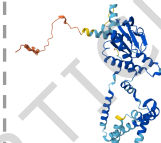


(694 aa)

STING



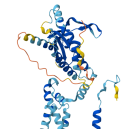
Length (384 aa)



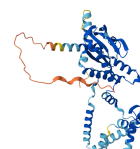
(382 aa)



(378 aa)



(379 aa)



(381 aa)

SURF4



Length (269 aa)



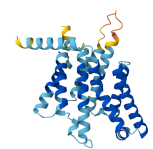
(269 aa)



(269 aa)



(256 aa)



(271 aa)